

Thesis

Machine Learning Modeling
and Parametric Assessment
of Rectangular Dielectric Reso-
nant Antenna

S. Chen

Technische Universiteit Delft

Thesis

Machine Learning Modeling and Parametric Assessment of Rectangular Dielectric Resonant Antenna

by

S. Chen

to obtain the degree of Master of Science
at the Delft University of Technology,
to be defended publicly on Tuesday October 9, 2018 at 13:00 AM.

Student number:	4587758
Project duration:	January 1, 2018 – October 1, 2018
Thesis committee:	Prof. dr. A. Yarovoy, TU Delft, supervisor
	Dr. ir. Bert-Jan. Kooij, TU Delft
	Dr. D. Tax, TU Delft
	Dr. J. B. Mills, Signify Company

This thesis is confidential and cannot be made public until October 31, 2023.

An electronic version of this thesis is available at <http://repository.tudelft.nl/>.

Signify Confidentiality Statement

The information contained in this thesis report may be confidential and/or legally protected under applicable law. The content is intended solely for the addressee(s). If you are not the intended recipient, you are hereby notified that any use, forwarding, dissemination, or reproduction of this report is strictly prohibited and may be unlawful. If you are not the intended recipient, please contact the author and destroy all copies of the original report.

Acknowledgment

This thesis becomes a reality under the help and kind support from many individuals. I would like to give my deepest appreciations to all of them.

In the university, I would like to thank my supervisor, Prof. A. Yarovoy for his guidance and insight to this thesis project. I also appreciate the technical supports from Pascal Aubry, Jan Puskely and Fred van der Zwan and suggestions from Wenjie Pei and Giannakis Iraklis.

In Signify, I would like to express my gratitude to my joint supervisor, Mr. Paul Boonen and my colleagues Dr. John Mills, Math Creemers, Dik Pardijs, Mai-han Truong and Jake.W.PRuijs. Thank them for their strong support, patience and caring during my whole internship.

I would also like to thank my parents and my friends Xiaoming Wen. They have been accompanying me for all the time.

Abstract

In recent years, researchers on dielectric resonant antennas (DRAs) have highlighted some of the attractive features. This type of antenna does not suffer from conduction losses like conductors and are characterized by high radiation efficiency when excited properly. The performance of a DRA is susceptible to various parameters, like dimensions, shapes, feeding options and the relative dielectric constant of the material. Estimating the performance of a DRA up to today is rather limited. Although some general methods, like FDTD and MOM, can work accurately, they sometimes cost too much time and require intensive compute processing and memory. With the development of artificial intelligence, the machine learning method starts to be applied in the electromagnetic field, creating a novel and efficient way to analyze the feasibility of a DRA for specific design requirements.

This thesis proposes constructing such a tool from the machine learning domain to realize a quick and precise way of estimating the performance of dielectric resonant antennas integrated in the lamps of Signify. The design range of the antenna parameters will be clarified according to the practical lamp products from the company. Within this range, the research aims at finding a suitable machine learning method and optimizing the learning model based on a priori simulation dataset. In this way, even non RF engineers can have a concept of the performance of the antenna before it is made. A proper dielectric resonant antenna for the Signify HUE lamp will be designed and estimated by the learning tool at the end of the thesis.

S. Chen
Delft, September 2018

List of Figures

2.1	Coaxial probe fed DRA[27]	5
2.2	Slot aperture feeding[27]	6
2.3	Microstrip feeding[30]	7
2.4	Co-planar waveguide feeding[27]	7
2.5	Diagrammatic sketch of cylindrical DRA[40]	8
2.6	Diagrammatic Sketch of Hemisphere DRA[34]	9
2.7	Dielectric waveguide[40]	10
2.8	RDRA with ground plane[40]	11
2.9	The transparent hemispherical DRA and the solar cell panel[37]	12
2.10	Transparent DRA made of glass[36]	13
3.1	The model of Kth neuron	16
3.2	Multiplayer feedforward network with one hidden layer and one output layer	17
3.3	Signal flow of output neuron k	17
3.4	Description for binary classification problem (adopted from [10]): (a) Two different groups of spots; (b) Divide spots by hyperplane A; (c) Divide spots by hyperplane B	20
3.5	Computation of the separation margin(adopted from [10])	21
3.6	Non-separable Patterns	22
3.7	Description for linear regression problem of SVM (adopted from [10])	23
4.1	Two-dimensional normalized power pattern (in dB, adopted from [47])	25
4.2	Antenna directivity calculation by antenna beam solid angles[12]	26
4.3	Thevenin equivalent circuit of antenna transfer mode[12]	28
4.4	Schematic diagram of rectangular DRA structure	29
4.5	Dimensions of the antenna ground plane	30
4.6	Simulation model and its waveguide port of RDRA (Construct on CST microwave studio 2018)	31
4.7	Structure diagram of neural network created by Matlab 2018a	33
4.8	How S11 of RDRA distribute with changing H and L	34
4.9	The prediction results on S11 of support vector regression model	34
4.10	The performance of neural network 1.0 version	35
4.11	The test results of neural network 1.0 version	37
4.12	The test results of neural network 2.0 version	38
4.13	The distribution diagram of training data	39
4.14	Mean error of test data (S11) for neural network version 3.0	39
5.1	Dielectric cubes and PCBs of DRA prototypes	44
5.2	Launch end connector 1092-01A-5 from Southwest Microwave	44
5.3	Converter between coaxial input and antenna PCB: (a) GCPW sketch ([9]); (b)CST model of the the converter circuit; (c)S parameter (S11: magnitude in dB) of the converter circuit	45
5.4	RDRA prototype for measurement	45
5.5	Radiation patterns in H cut of ten RDRA prototypes	47
5.6	Comparison of NN prediction, CST simulation and measurements for RDRA prototypes: (a) Comparison result of S11; (b) Comparison result of HPBW	48

List of Tables

4.1	Input features setting of the learning model	30
4.2	The test dataset for the learning machine: (a) the S11 satisfies: $S_{11} < -15$ dB; (b) the resistance R_A satisfies: $40 < R_A < 60$ Ohm; (c) the reactance satisfies: $-20 < X_A < 20$ Ohm; (d) the HPBW satisfies: HPBW > 60 degree	32
4.3	Mean error of test data for neural network version 1.0	36
4.4	Mean error of test data for neural network version 2.0	36
4.5	Mean error of test data for neural network version 3.0	40
4.6	Structure and performance of the final neural network	40
5.1	The dimensions of resonator cubes in measurements	43
5.2	The dimensions of ground plane in measurements	44
5.3	Measurement results of RDRA prototypes ($\epsilon_r = 2.55, L_{stub} = 2.3mm$)	46

Contents

List of Figures	vii
List of Tables	ix
1 Introduction	1
1.1 Motivation	1
1.1.1 Application Background	1
1.1.2 Dielectric Resonator and Machine Learning	1
1.1.3 Objective of Thesis	2
1.2 Thesis outline	2
2 Dielectric Resonant Antenna	5
2.1 Introduction	5
2.1.1 Excitation Methods	5
2.1.2 The Common geometries of the DRA	6
2.2 Rectangular Dielectric Resonant Antenna.	10
2.2.1 Dielectric Waveguide Model	10
2.2.2 Field Analysis in Rectangular DRAs	11
2.2.3 Resonant frequency and Q factor	11
2.2.4 Influence of finite ground plane	12
2.3 Transparent DRA: the Aesthetic Antenna	12
2.4 Conclusion	13
3 Machine Learning	15
3.1 Neural Network	15
3.1.1 Basic Structure of a Neural Network	15
3.1.2 Multilayer Feedforward Networks	16
3.1.3 Backpropagation Algorithm	17
3.1.4 Advantages of Neural Network	19
3.2 Support Vector Machine	19
3.2.1 Linearly Separable Patterns	20
3.2.2 Non-separable Pattern	21
3.2.3 Kernel Functions for SVM	22
3.2.4 Support Vector Regression	23
3.3 Conclusion	24
4 Learning Model for the RDRA Design	25
4.1 Design Space of Rectangular DRA.	25
4.1.1 Definitions of Antenna Parameters.	25
4.1.2 Practical Requirements on Antenna Parameters setting	28
4.1.3 The Collection and Classification of Data	30
4.2 Construction of the Training Model.	31
4.2.1 Requirements of the Learning Model	31
4.2.2 Neural Network Model	32
4.2.3 Support Vector Machine Model	33
4.2.4 Comparison between Two Models	33
4.2.5 A short summary.	36
4.3 Optimization of Training Model.	36
4.3.1 Separation of learning objects	36
4.3.2 Imbalance data distribution problem	36
4.4 Conclusion	40

5 Experiment Verification	43
5.1 RDRA Prototype Design	43
5.1.1 Design of Rectangular DRA	43
5.1.2 Design of Grounded Co-planar Waveguide.	44
5.2 Measurement Results and Analysis	45
5.3 Conclusion	48
6 Conclusion and Future Work	49
6.1 Conclusion	49
6.2 Future Work.	49
Bibliography	51



Introduction

1.1. Motivation

1.1.1. Application Background

Signify has been looking for the proper sensors that can be integrated in their LEDs lamps. In this way, they can achieve the purpose to produce intelligent lighting products, which can control the level of illumination depending on the detected human motion. For consumers, they can construct their own wireless lighting system at home to enjoy a smarter and more convenient life. For environment, more energy can be used wisely and saved by wireless control, since the microwave sensor can help to adjust the light automatically according to human activities. It will never forget to turn the bulbs off if no one is at home.

They have made lots of interesting attempts, like passive infrared sensor(PIR), ultrasound sensors and VGA camera. However, these choices have irreparable drawbacks. PIR and ultrasound sensor call for a window on the bulb housing so that the signal can be transferred, which may violate the IP code(International Protection Rating[52]) that the company has to obey. If so, the company needs to pay more money on redesigning other parts in the bulb to fix this problem. For the VGA camera, things become even more complicated. The camera cannot be integrated in a bulb, causing more troubles for bulb installing process. Besides, the data processing task for such a camera is heavy as well as expensive. Of course, camera is also likely to violate privacy regulations.

They finally looked into microwave sensors for their good ability in detecting human motion plus it can be fixed within a closed bulb environment. A crucial part of the microwave sensor is the antenna. Based on the antenna topology comparison work which had been done by Miss Mai-han Truong and the author during their internship in the company, the dielectric resonant antenna, which will be illustrated in next chapter, was chosen for this application.

1.1.2. Dielectric Resonator and Machine Learning

Dielectric resonant antennas DRA have attracted attention for a long time. For many years, the dielectric resonators were mainly used for oscillators and filters in microwave circuits[25]. In these applications, the material of dielectric resonators always have a high permittivity and Q-factor. That's why the dielectric resonator used to be treated more as energy storage. Using the dielectric resonator(DR) as antenna was widely accepted from around 30 years ago. At that time, with the frequency of interest increasing constantly, people started to find the metallic antenna suffering from serious conduction losses. Also, the antenna efficiency drops severely in the millimeter wave range[40]. Conversely, dielectric material has some attractive qualities in these aspects. Due to the dielectric, the wavelength is reduced by a factor of $1/\sqrt{\epsilon_r}$ compared to the wavelength in free space. The dielectric material also implies the possibility of designing smaller antenna. From that time on, research is boosted in the DRA.

The DRA, like other microwave components, is traditionally analyzed and designed by electromagnetic numerical methods, which is a time consuming, as well as computationally expensive work. From the end of the 1990s, machine learning computational modules started to be recognized as a novel and useful tool for RF and microwave modeling and design[58]. Machine learning was first named in 1959 by Arthur Samuel. After a dormant period, machine learning was accepted as a separate field and started to flourish in the 1990s. It combines calculations and data retrieval to make the computer system appear to be learning and making

rational decisions according to previously knowledge and experience[50].

In the area of antenna design, the concept of machine learning can also be applied. Training a "machine" to learn the behavior of an antenna under different design requirements can provide fast answers. After the proper model has been constructed, a quick estimation about antenna performance can be attained. Then, later simulation and optimization work about the antenna design can be more targeted.

1.1.3. Objective of Thesis

The main goal for this thesis is to exploit the idea from the machine learning domain[19] to analyze the feasibility of creating a computationally efficient model for predicting circuit and radiation parameters of a dielectric resonant antenna.

As it is introduced in the former section, dielectric resonant antenna will be applied in the lamp application. However, the performance of a DRA is susceptible to various parameters, like the antenna dimensions, shapes, feeding options and relative dielectric constant of the material[27]. Especially at high frequencies, antennas are even more sensitive to the changes of those parameters. On the other hand, the working environment within the bulb housing varies between the different types of bulb. The truth is that Signify possesses so many different kinds of bulbs, with diverse shapes, inner structures and LEDs array configurations. Even the same series of bulbs may be redesigned to a newer version afterwards. Under this condition, it can be assumed that the DRAs in each kind of bulbs have to be identical. This brings some problems. Dielectric resonant antenna, which will also be mentioned in subsequent chapters, cannot be designed directly by any explicit functions up to now. The full-wave electromagnetic analysis in the DR is quite difficult, requiring complicated as well as long-duration simulations and optimizations.

In order to simplify the antenna design process for the potential lamp configurations, the company would first like to obtain a dataset containing possible antenna parameters. In this way, they can easily find the relative antenna parameters, avoiding the design process which asks for professional antenna knowledge and design skills. However, since the DRA is very sensitive at such a high frequency(24GHz), as mentioned before, even slight changes in the DRA may make a big difference on its final performance. So, if the dataset is desired to be qualified for most of the antennas that are integrated in their lamp production, the amount of data collected beforehand by simulation and optimization is huge. In other words, to create such a dataset is extremely time consuming and expensive.

Hence, a more efficient method, which can help to assess the antenna performance in the future design, but does not ask for a complete data base, is the numerical performance prediction model. This inspires the thesis to apply the machine learning method in the field of antenna. Machine learning is widely employed in computing tasks when designing and programming explicit algorithms with good performance is infeasible[53]. This is exactly what is wanted in this situation. The idea to apply the machine learning method in electromagnetics(EM) is not unique to this thesis and some researchers have already proven that this technique can be utilized to solve EM design problems, including antenna array, frequency selective surfaces and filters etc[11]. Yet it is the first time it has been used to estimate and analyze the DRA performance under diverse and complicated design space by using the machine learning method in this thesis.

1.2. Thesis outline

The thesis will be constructed according to outline below:

- **Chapter 1**

A general introduction to the thesis. The objective of this thesis is specified in this chapter, as well as goals of research and approach.

- **Chapter 2**

In this chapter, the basic theory of DRAs is presented. Based on relative literatures, the excitation methods, common geometries and field analysis of DRAs will be specified. After this, more details about rectangular DRAs will be given, since for the later research, rectangular DRAs are the main object of this thesis. The last section is about the transparent DRA, showing the possibility of employing DRAs as a part of optical device in practical application.

- **Chapter 3** This chapter is all about machine learning. The fundamental concepts of machine learning will be shown in the first section, followed by two important learning techniques, neural network and

support vector machine. Furthermore, some examples and instructions about how to apply machine learning in EM aspect will be given.

- **Chapter 4** This chapter describes the construction process of the machine learning model. The design space of the DRA will be specified at first. Within this scope, neural network learning model and support vector machine model are built respectively. Their training results will be compared so that the better one for this application can be chosen. The optimization of the preferred model will also be displayed afterwards.
- **Chapter 5** This chapter is focused on the experimental verification results. Real antenna prototypes will be designed in this part and their performances will be measured in laboratory. Measurement results will be used to test the reliability of the simulation and learning model.
- **Chapter 6** Conclusions and reflections of the thesis project are presented in final chapter, as well as the suggestion for future work.

2

Dielectric Resonant Antenna

2.1. Introduction

2.1.1. Excitation Methods

There are various options for feeding the DRA, which enables more possibilities in designing a DRA. In this part, the mostly common used excitation techniques will be introduced.

Coaxial Probe-Fed DRA

Fed by coaxial probe is one of the earliest methods to excite DRA[43]. The configurations of this excitation method are shown in figure 2.1. The dielectric resonators are placed on the ground plane directly. Meanwhile, the coaxial probe can be inserted into the DR (shown in figure2.1(a)) or be placed so as to attach to one surface of the DR.

The first configuration has the advantage of better radiation efficiency, due to the good coupling between the probe and DR. But drilling holes in the resonator also causes some problems. If the dimensions of the holes do not match to the probes perfectly, air gap between resonator and probe may influence the effective dielectric constant of the resonator. As a result, the resonance frequency of the antenna may be shifted. Besides, the manufacturing process also becomes more difficult, which means the cost of production goes up. On the other hand, placing the probe adjacent to the DR can make manufacturing easier and cost less money. However, the drawback is the poorer coupling between the coaxial probe and the DR.

For both configurations, adjusting the lengths or positions of the probes, the input impedance of the DRA can be changed. This is the way to control the resonance frequency of the DRA. But for high-frequency applications, where the circuits are highly integrated, this excitation method is not very practical.[27]

Aperture Coupling Feeding

Aperture coupling feeding is another very popular method. Although the figure 2.2 shows a cylindrical DRA, this excitation technique can be used for DRA of all shapes. The DR is deposited on the ground plane, below

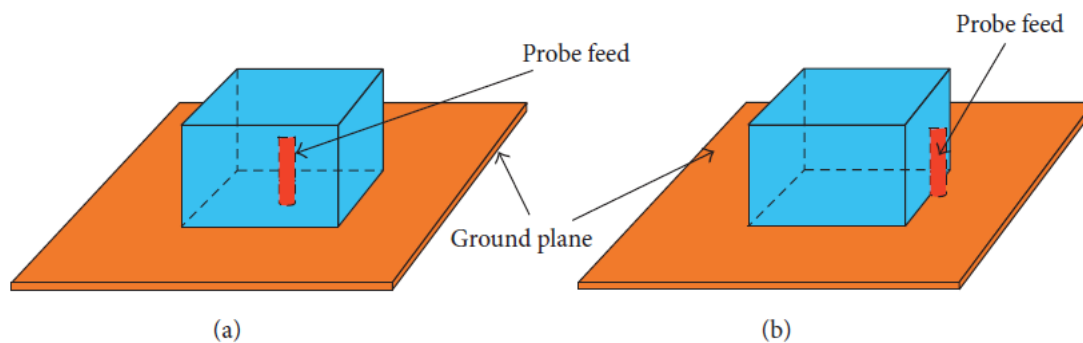


Figure 2.1: Coaxial probe fed DRA[27]

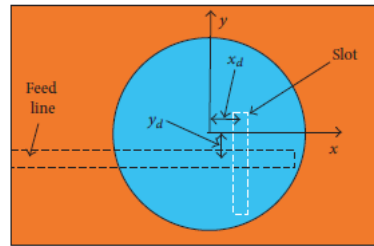


Figure 2.2: Slot aperture feeding[27]

which is the substrate. Microstrip feed line is at the lowest layer. Through the slot aperture, the guided wave along the feed line is coupled to the resonant modes of the DR. The analysis about how the displacement of the DR effects the aperture coupling can be found in [35]. It was proved that the best coupling is achieved when the DR is centered at the top of the slot center. In addition, adjusting the microstrip stub properly can cancel out the reactive component of the slot, resulting in the impedance matching to the DRA.

Aperture coupling avoids direct electromagnetic interaction between the DRA and feed line. The DR can be regarded as a kind of waveguide in this topology, thus, the spurious radiation will be reduced, leading to the higher polarization purity of the DRA. However, this method also has its own drawbacks. It is well known that the slot length should be around half wavelength at the working frequency. Then if the antenna works at low frequency, it will be very challenging to make a circuit compact due to the long slot[28].

Direct Feeding by Microstrip Line

Feeding the DRA directly by microstrip line is also equally applicable to DRAs of all topologies as it is shown in figure 2.3, Below the DR, the circuit can be deemed as a microstrip antenna. The microstrip coupling will excite the magnetic fields in the DR to produce a short horizontal magnetic dipole mode. The coupling level between the transmission line and the DR is dependent on the permittivity of the DR and how much the DR overlaps the transmission line. For lower permittivity, the coupling level is not very high and the radiation efficiency is not ideal either. In order to have a better coupling, a DRA array is needed. For a linear DRA array, the transmission line can feed them in series. The disadvantage is that the polarisation of the array is influenced by the orientation of the microstrip line[30].

Co-planar Waveguide Feeding

The last common feeding method that will be introduced here is co-planar waveguide(CPW) excitation. There is an example shown in figure 2.4. This method was first reported in [31]. This CPW under the DR can be modified in many ways, like adjusting its size and shape, to realize the optimization of the DRA's performance. In [18], the author replaced the circle CPW with inductive slot and capacitive slot.(shown in figure 2.4(b),(c)). It is proved that the capacitive slot can provide an additional resonance which causes a dual-band behavior. This may be applied for multiple frequencies of application. Currently, CPW feeding technique is used for many millimeter-wave applications, especially for those being integrated in a system on chip (SoC). Since the ground plane separates the DR from the lossy silicon substrate, the antenna efficiency can be quite high in this situation.[27]

2.1.2. The Common geometries of the DRA

With the suitable excitation method, any dielectric resonator can become a radiator, working as an antenna at the desired frequency. Various shapes of the DRA can also effect the radiation performance of the antenna. Three shapes of the DRA, which is the most basic and commonly used, are introduced in this section. They are the cylindrical DRA(CDRA), hemisphere DRA(HDRA) and rectangular DRA(RDRA). The analysis of their field mode configurations, resonant frequency and radiation pattern etc. will also be illustrated[40].

Cylindrical DRA

Cylindrical DRA (CDRA) offers great design flexibility. The resonant frequency and the Q factor are controlled by the height and the radius of the CDRA. In [39], the brief analysis of the field excited in the DRA is given.

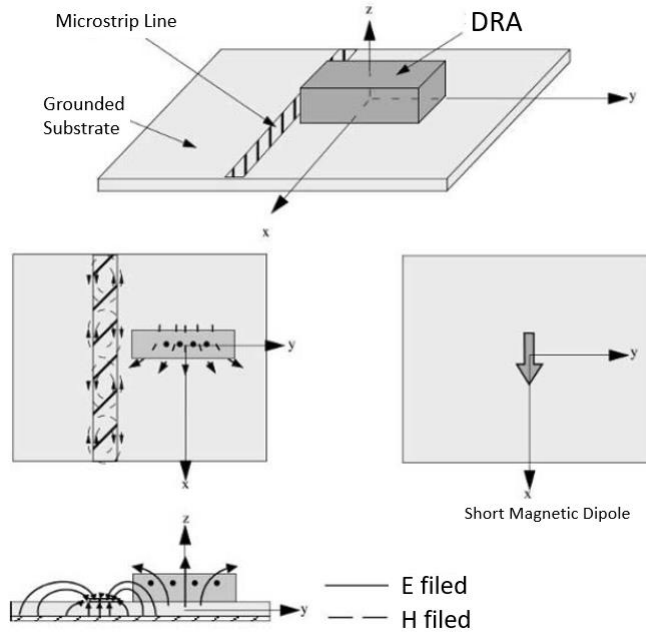


Figure 2.3: Microstrip feeding[30]

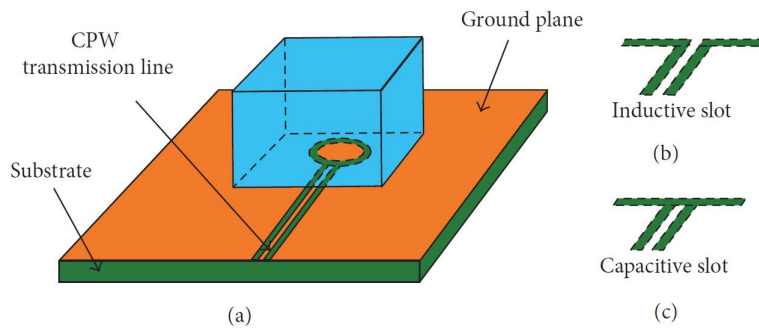


Figure 2.4: Co-planar waveguide feeding[27]

Resonant frequency: The topology of the CDRA is shown in figure 2.5 and a relative coordinator is built there. Image theory is applied in this situation and the surfaces of the DRA can be assumed to be perfect magnetic conductors, where the feed probe is ignored temporarily. In this case, wave functions which are transverse electric (TE) to z and transverse magnetic (TM) to z are:

$$\psi_{TE_{n\phi m}} = J_n \left(\frac{X_{np}}{a} \rho \right) \begin{pmatrix} \sin n\phi \\ \cos n\phi \end{pmatrix} \sin \left[\frac{(2m+1)\pi}{2d} z \right] \tag{2.1}$$

$$\psi_{TM_{n\phi m}} = J_n \left(\frac{X'_{np}}{a} \rho \right) \begin{pmatrix} \sin n\phi \\ \cos n\phi \end{pmatrix} \sin \left[\frac{(2m+1)\pi z}{2d} \right] \tag{2.2}$$

where the J_n is the Bessel function of the first kind. Combined with the separation equation $k_\rho^2 + k_z^2 = k^2 = \omega^2 \mu \epsilon$, the resonant frequency of the n ϕ m mode can be written as:

$$f_{n\phi m} = \frac{1}{2\pi a \sqrt{\mu \epsilon}} \sqrt{\left(\frac{X_{np}^2}{X_{np}'^2} \right) + \left[\frac{\pi a}{2d} (2m+1) \right]^2} \tag{2.3}$$

In practical applications, the most attractive mode is the fundamental mode, which has the lowest resonant

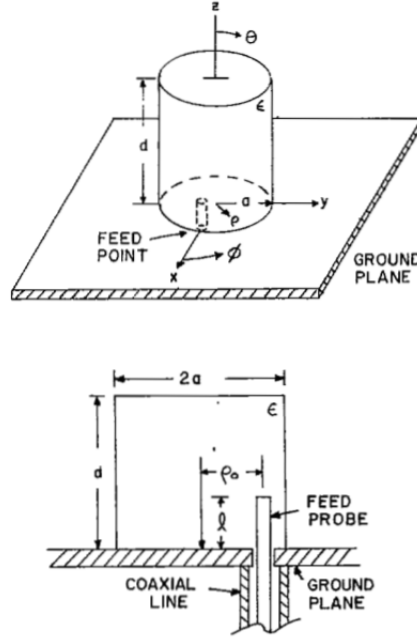


Figure 2.5: Diagrammatic sketch of cylindrical DRA[40]

frequency. In the CDRA, the fundamental mode is the TM_{110} mode, whose resonant frequency is:

$$f_{TM_{110}} = \frac{1}{2\pi a \sqrt{\mu\epsilon}} \sqrt{X'_{11}{}^2 + \left(\frac{\pi a}{2d}\right)^2} \quad (2.4)$$

where $X'_{11}{}^2$ equals 1.841.

Far-field pattern: The spherical coordinator of the CDRA is shown in figure 2.5. The far field of the fundamental mode TM_{110} is discussed in this part. Based on equation 2.2, the wave function of the TM_{110} mode is found:

$$\psi_{TM_{110}} = J_1\left(\frac{X'_{11}\rho}{a}\right) \cos\phi \cos\frac{z\pi}{2d} \quad (2.5)$$

From the wave function, the E-fields can be found:

$$E_\phi = \frac{1}{j\omega\epsilon\rho} \frac{\partial^2\phi}{\partial\phi\partial z}, \quad E_z = \frac{1}{j\omega\epsilon} \left(\frac{\partial^2}{\partial z^2} + k^2\right)\phi, \quad E_\rho = \frac{1}{j\omega\epsilon} \frac{\partial^2\phi}{\partial\rho\partial z} \quad (2.6)$$

The magnetic currents on the CDRA surface can then be found by applying the equivalence principle. Through $\vec{M} = \vec{E} \times \hat{n}$, where the \hat{n} is a unit normal of the DRA surface and points to the surface outside. Then the magnetic currents(for the side wall) can be expressed as:

$$M_{z'} = \frac{\rho i}{2j\omega\epsilon a d} j_1(X'_{11}) \sin\phi' \sin\frac{\pi z'}{2d} \quad (2.7)$$

$$M_{\phi'} = \frac{1}{j\omega\epsilon} \left(\frac{X'_{11}}{a}\right)^2 \cos\phi' \cos\frac{\pi z'}{2d} \quad (2.8)$$

Now, the far field can be explored based on the above derivation of the currents. In the spherical coordinates(r, θ, ϕ),the source currents are interpreted as:

$$M_\theta = M_{\rho'} \cos\theta \cos(\phi - \phi') + M_{\phi'} \cos\theta \sin(\phi - \phi') - M_{z'} \sin\theta \quad (2.9)$$

$$M_\phi = -M_{\rho'} \sin(\phi - \phi') + M_{\phi'} \cos(\phi - \phi') \quad (2.10)$$

Then the electric vector potentials can be computed as:

$$F_\theta = \frac{e^{-jk_0 r}}{4\pi r} \iiint M_\theta e^{jk_0[\rho' \sin\theta \cos(\phi-\phi') + z' \cos\theta]} \rho' d\rho' d\phi' dz \quad (2.11)$$

$$F_\phi = \frac{e^{-jk_0 r}}{4\pi r} \iiint M_\phi e^{jk_0[\rho' \sin\theta \cos(\phi-\phi') + z' \cos\theta]} \rho' d\rho' d\phi' dz \quad (2.12)$$

where $k_0 = \omega\sqrt{\mu_0\epsilon_0}$ is the wavenumber in free space. In far field region, the electric fields E_θ , E_ϕ are proportional to the electric vector potentials F_ϕ , F_θ respectively.

Many other researchers also devoted a lot to the analysis of the CDRA, like Shum and Luk applied the finite-difference time domain(FDTD) method in[48]. Gregory P. Junker used the body of revolution(BOR) method to analyze the CDRA[24].

Hemisphere DRA

Compared to the rectangular DRA, the hemisphere DRA has a simpler interface between the DR and air, which makes it easier to analyze the field by Green's function. The configuration of the hemisphere DRA is shown in

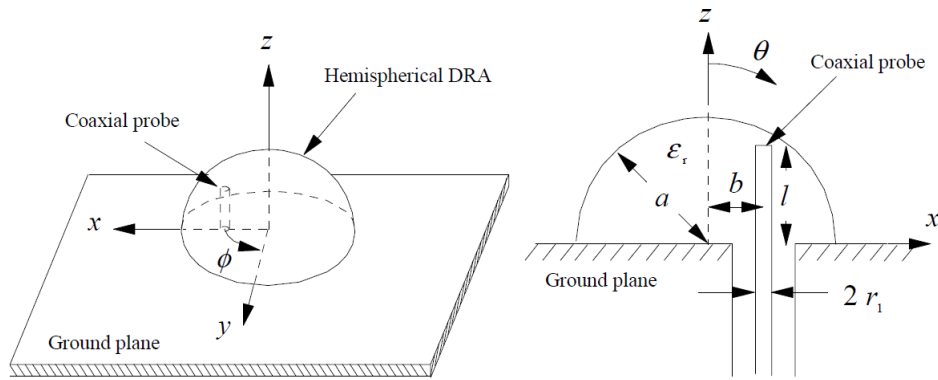


Figure 2.6: Diagrammatic Sketch of Hemisphere DRA[34]

figure 2.6. This HDRA is fed by the coaxial probe. In the coordinator, the field is denoted by $\vec{r}(r, \theta, \phi)$ and the source point is represented by $\vec{r}'(r', \theta', \phi')$. The single mode TE_{111} will be discussed as an example in next paragraph and more details about the field analysis can be found in [34].

TE_{111} mode analysis: The single-mode approximation[33] and image theory are applied in the analysis. Then the Green's function of the E-field in the spherical coordinator is:

$$G_{TE_{111}} = \frac{-3k}{8\pi\omega\epsilon_r r'} \sin\theta \sin\theta' \cos(\phi - \phi') [\Phi(kr)\Psi(kr) + \alpha_{TE} \hat{J}_1(kr') \hat{J}_1(kr)] \quad (2.13)$$

where

$$\Phi(kr) = \begin{cases} \hat{J}_1(kr'), & r > r' \\ \hat{H}_1^{(2)}(kr'), & r < r' \end{cases}, \quad \Psi(kr) = \begin{cases} \hat{H}_1^{(2)}(kr), & r > r' \\ \hat{J}_1(kr), & r < r' \end{cases} \quad (2.14)$$

$$\alpha_{TE} = \frac{-1}{\Delta_{TE}} [\hat{H}_1^{(2)}(ka) \hat{H}_1^{(2)'}(k_0 a) - \sqrt{\epsilon_r} \hat{H}_1^{(2)'}(ka) \hat{H}_1^{(2)}(k_0 a)] \quad (2.15)$$

$$\Delta_{TE} = \hat{J}_1(ka) \hat{H}_1^{(2)'}(k_0 a) - \sqrt{\epsilon_r} \hat{J}_1'(ka) \hat{H}_1^{(2)}(k_0 a) \quad (2.16)$$

In the above equations, $k_0 = \omega\sqrt{\mu_0\epsilon_0}$, $k = \sqrt{\epsilon_r} k_0$. $\hat{J}_1(X)$ and $\hat{H}_1^{(2)}(x)$ are the first-order spherical Bessel function of the first kind and spherical Hankel function of the second kind respectively. Applying the Green's function, the electric field E_z excited by the probe current J_z can be found:

$$E_z(\vec{r}) = \iint_{S_0} G_{TE_{111}}(\vec{r}, \vec{r}') J_z(z') dS' \quad (2.17)$$

and

$$J_z(z') = J_0 \text{sinc}(l - |z'|), \quad -l \leq z \leq l \quad (2.18)$$

J_z is the surface current which is assumed flowing on the imaged probe surface S_0 . With the surface current, the input impedance of the antenna can be determined by applying the variation formula. In[40], the theoretical results of the impedance are compared with the measurement made by McAllister and Long[42].

Rectangular DRA

The rectangular DRA (RDRA) is also very commonly-used in practical life. Although the theoretical analysis of the RDRA is even more difficult than the other two shaped DRA that are introduced before, the RDRA provides practical advantages over cylindrical and hemispherical DRAs. The RDRA is characterized by three independent geometrical dimensions, giving more possibilities of designing compared to the CDRA and the HDRA. The mode degeneracy can be avoided if the three dimensions of the RDRA are properly chosen. In the case of a spherical DRA and a cylindrical DRA, the mode degeneracy or hybrid modes always exist.[44]. Combined with the scope of the application that is mentioned at the beginning of this report, the RDRA will be mainly studied and applied for the rest of the thesis. More details and research about the RDRA will be specified in the next section. Hence it will not be explored here.

2.2. Rectangular Dielectric Resonant Antenna

Theoretically, analysis of the RDRA is more difficult than the cylindrical and hemispherical DRA due to the edge shaped boundaries. The dielectric waveguide model is usually applied to solve this problem. Shum and Luk[49] used a more accurate approach, the FDTD method, to analyze the aperture-coupled RDRA, but the time cost is higher, also requiring intensive memory. In the next part, the dielectric waveguide method will be mainly discussed.

2.2.1. Dielectric Waveguide Model

In [41], the dielectric waveguide model was first came up for determining the guided wavelength in dielectric with rectangular cross-section. The sketch of the dielectric waveguide and the field distribution on its cross section are shown in figure 2.7. It defines the width a in the x -direction, height b in the y -direction and waves propagating in the z -direction. TE_{mn}^y and TM_{mn}^y denote the field modes in the guide, where m and n stand for the number of field extrema in the x -direction and y -direction respectively. The fields in the guide are supposed to vary sinusoidally and the fields outside the guide are decay exponentially.

Then based on figure 2.7, the wave propagation numbers in each direction and the attenuation constants in the x and y directions can be determined.

$$k_z = \sqrt{\epsilon_r k_0^2 - k_x^2 - k_y^2} \quad (2.19)$$

$$k_x = \frac{m\pi}{a} \left(1 + \frac{2}{ak_0\sqrt{\epsilon_r - 1}} \right)^{-1} \quad (2.20)$$

$$k_y = \frac{n\pi}{b} \left(1 + \frac{2}{bk_0\sqrt{\epsilon_r - 1}} \right)^{-1} \quad (2.21)$$

$$\alpha = \frac{1}{\sqrt{(\epsilon_r - 1)k_0^2 - k_x^2}} \quad (2.22)$$

$$\gamma = \frac{1}{\sqrt{(\epsilon_r - 1)k_0^2 - k_y^2}} \quad (2.23)$$

In above equations 2.19, the subscriptions denote the directions of the wave propagation numbers within the guide. α and γ are the attenuation constants in the x and y directions respectively. k_0 is the wave number in the free space which can be expressed as:

$$k_0 = \frac{2\pi}{\lambda_0} = \frac{2\pi f_0}{c} \quad (2.24)$$

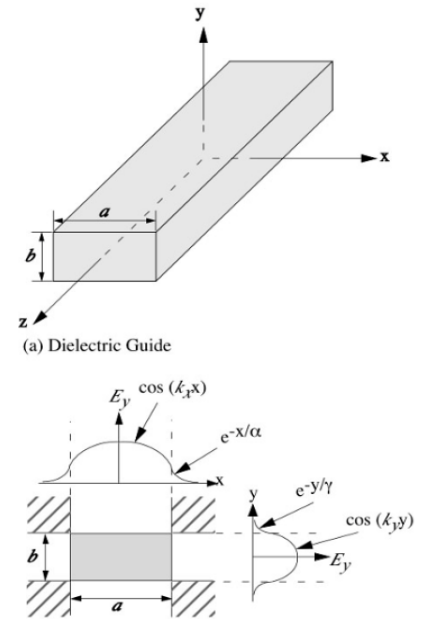


Figure 2.7: Dielectric waveguide[40]

where c is the speed of light in the free space, λ_0 is the wavelength in the free space and f_0 is the working frequency.

2.2.2. Field Analysis in Rectangular DRAs

The dielectric waveguide theory can be applied to solve the RDRA problem now. The orientation of the RDRA needs to be specified here. The width of the tube is along x direction, named " a ". The length " d " is along z direction, while the height " h " is along y axis. Different from figure 2.7, the height of the RDRA is only half of " b " ($h = \frac{1}{2}b$) due to the ideal ground plane. If the dimensions of the DRA obey the rule that $a, b > d$, the

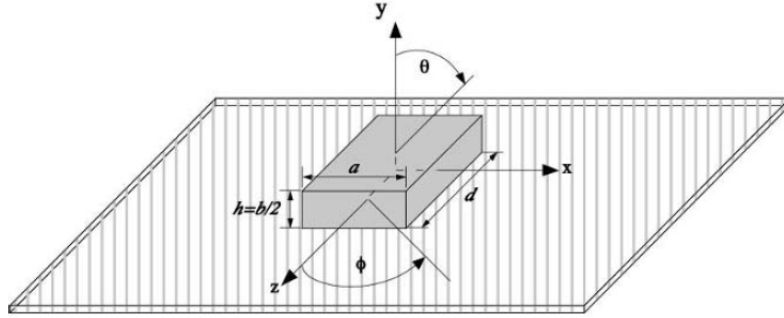


Figure 2.8: RDRA with ground plane[40]

lowest order mode will be $TE_{11\sigma}^z$. The fields within the DRA are like[44]:

$$H_x = \frac{(k_x k_z)}{j\omega\mu_0} \sin(k_x x) \cos(k_y y) \sin(k_z z) \quad (2.25)$$

$$H_y = \frac{k_y k_z}{j\omega\mu_0} \cos(k_x x) \sin(k_y y) \sin(k_z z) \quad (2.26)$$

$$H_z = \frac{k_x^2 + k_y^2}{j\omega\mu_0} \cos(k_x x) \cos(k_y y) \cos(k_z z) \quad (2.27)$$

$$E_x = k_y \cos(k_x x) \sin(k_y y) \cos(k_z z) \quad (2.28)$$

$$E_y = -k_x \sin(k_x x) \cos(k_y y) \cos(k_z z) \quad (2.29)$$

$$E_z = 0 \quad (2.30)$$

Besides,

$$k_x^2 + k_y^2 + k_z^2 = \epsilon_r k_0^2 \quad (2.31)$$

$$k_z \tan(k_z \frac{d}{2}) = \sqrt{(\epsilon_r - 1)k_0^2 - k_z^2} \quad (2.32)$$

2.2.3. Resonant frequency and Q factor

From the equations above, the resonant frequency of the RDRA can be found according to the wave numbers on each direction (k_x , k_y and k_z). Here, the fundamental mode TE_{111} is specified as an example[45]:

$$f_0 = \frac{c}{2\pi\sqrt{\epsilon_r}} \sqrt{k_x^2 + k_y^2 + k_z^2}$$

$$k_x = \frac{\pi}{a}$$

$$k_y = \frac{\pi}{2h} \quad (2.33)$$

$$d = \frac{2}{k_z} \tanh\left(\frac{k_z d}{2}\right)$$

$$k_{y0} = \sqrt{k_x^2 + k_z^2}$$

In [44], the radiation Q-factor of the RDRA is:

$$Q = \frac{2\omega W_e}{P_{rad}} \quad (2.34)$$

W_e is the stored energy and P_{rad} is the radiated power. They can be computed by:

$$W_e = \frac{\epsilon_0 \epsilon_r abd}{32} \left(1 + \frac{\sin(k_z d)}{k_z d} \right) (k_x^2 + k_y^2) \quad (2.35)$$

$$P_{rad} = 10k_0^4 |p_m|^2 \quad (2.36)$$

and the magnetic dipole p_m is:

$$p_m = \frac{-j8\omega\epsilon_0(\epsilon_r - 1)}{k_x k_y k_z} \sin\left(\frac{k_z d}{2}\right) \hat{z} \quad (2.37)$$

Then from the radiation Q-factor, the impedance bandwidth of the RDRA can be estimated as:

$$BW = \frac{S - 1}{Q\sqrt{S}} \quad (2.38)$$

The "S" in the equation 2.38 is the maximum acceptable voltage standing wave ratio (VSWR).

2.2.4. Influence of finite ground plane

Until now, all the computations and equations about the RDRA are made on the assumption that the RDRA is placed on an infinite ground plane. However, this is just too ideal to believe for the practical applications. Radiation patterns of these applications are influenced by the scattering wave from the edges of a finite ground plane. For a small ground plane, numerical methods can be applied to predict the effect of the scattering wave (with ground plane $\sim 1\lambda$). But when the size of ground plane increases, numerical method becomes less useful due to computer memory requirements. Geometric Theory of Diffraction is used more for large ground plane (with the size $\sim 8\lambda$ to 10λ) [40]. If the ground plane size extends beyond 10λ , the scattering effect can be ignored normally.

2.3. Transparent DRA: the Aesthetic Antenna

In [37], the optical function of transparent DRA is firstly proposed. The author made the hemispherical DRAs out of Borosilicate Crown glass (Pyrex), which is a kind of transparent dielectric material. This hemispherical dielectric resonator not only serves as a part of the antenna, but also provides the function of a lens in figure 2.9. The focusing lens allows the light to pass through it and illuminates the solar cell that is under the DR. In

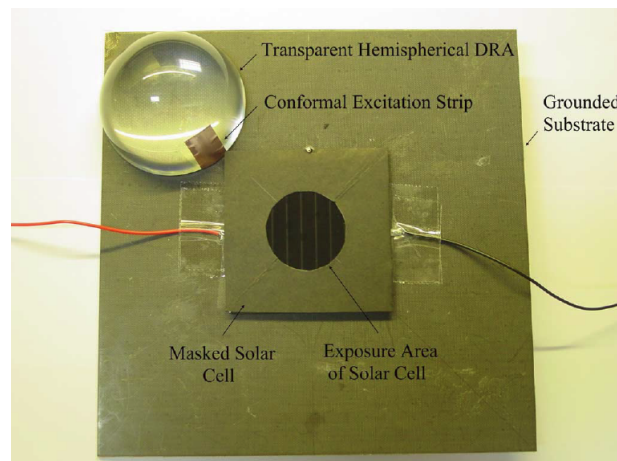


Figure 2.9: The transparent hemispherical DRA and the solar cell panel [37]

other words, the focusing effect of the DRA can help to improve the Voltage and Current outputs of the solar cell. Thus, the circuit can be quite compact since no extra footprint is needed for the solar cell.

Another application of the transparent DRA, which is also the main application that this thesis studies, is to be a light source. As it is mentioned in the beginning of this thesis report, the antennas that the company desire are those that can be integrated in the lamp without affecting the illumination. In [36], there is a successful example applying the transparent antenna in this case. As it is shown in the figure 2.10, the clear lamp cover is



Figure 2.10: Transparent DRA made of glass[36]

also used as the dielectric resonator of the DRA. Also in [36], the group of Prof. Kwok Wa Leung manufactured some decorative antennas based on crystal and glass material. These beautiful antenna artworks are potential in the situation where the standalone or visible antennas are not wanted.

2.4. Conclusion

In this chapter, brief structure of dielectric resonant antenna has been introduced firstly, including its common excitation methods and geometries. Rectangular DRA fed by slot aperture is chosen as the targeted topology for this thesis. Because the design of RDRA has a relatively wide degree of freedom and it is low cost in manufacturing. What's more, the existence of transparent dielectric material makes the DRA more applicable to the application that mentioned in the Chapter 1.

Then from the analysis of the fields distributed in the RDRA, the difficulties and computation loads of designing the RDRA are displayed. Besides, the miss of completely accurate analyzed model and the influence from finite ground plane make theoretical computation results of the RDRA become less reliable. This stresses the motivation and importance to develop an artificial intelligent model which can provide a fast and accurate estimation of the RDRA.

3

Machine Learning

In this thesis, two popular machine learning methods are proposed to build the model. They are Neural Network (NN) and Support Vector Machine (SVM). This chapter represents the study of the structure and working principles of these two methods.

3.1. Neural Network

Artificial neural network(ANN) is motivated by the information processing system in human brains. Human brains are capable of organizing neurons to perform highly complex, nonlinear and parallel computation in an extremely effective way. Take our visual ability as an example, people can recognize the face of an acquaintance easily in a totally unfamiliar environment, which can be accomplished within 200 ms. No existing computer, even the most powerful one, can achieve this computation speed.[19]

Many researchers have put effort on simulating the neuron system in the human brains. Back to the late 1940s, Hebbian learning[21], a learning method suggested by D.O.Hebb, was created based on "neuron plasticity" [56]. In 1958, Rosenblatt created the perceptron algorithm [46] and he described circuitry with mathematical notation. Until the year of 1965, the first functional multi-player network was put forward by Ivakhnenko and Lapa. However, the development of neural network was retained due to the low processing power of the computer at that time. After 1975, Werbos's backpropagation algorithm redrew the research attention back to neural network. Until the end of 1990s, Simon Haykin clearly defined neural network in the book *Neural Network and Learning Machine*[19] as:

"A neural network is a massively parallel distributed processor made up of simple processing units that has a natural propensity for storing experiential knowledge and making it available for use. It resembles the brain in two respects:

- 1. Knowledge is acquired by the network from its environment through a learning process;*
- 2. Interneuron connection strength, known as synaptic weights, are used to store the acquired knowledge."*

3.1.1. Basic Structure of a Neural Network

Neuron Model

The fundamental unit of an ANN is a neuron. The basic nonlinear structure of the Kth neuron in an ANN is shown in figure 3.1. In order to mimic a biological neuron[55], the artificial neural model should has three basic elements:

- **Synapses** are the connecting links of a neuron. Each synapse has its own weight ω . The input signal x_m of the synapse m multiplies the weight ω_{km} .
- **An adder** is used to sum up the weighted input signals.
- **An activation function** $\varphi(\cdot)$, also called as squashing function, which can limit the neuron output amplitude.

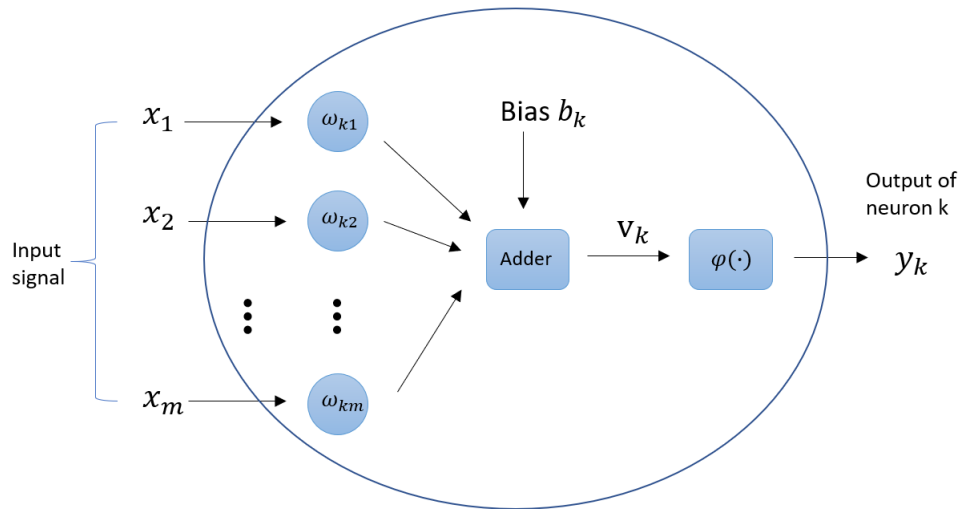


Figure 3.1: The model of Kth neuron

Besides, the bias b_k in neuron k can modulate the range of the input of the activation function. The mathematical relationship between the output and input of the neuron k can be written as:

$$y_k = \varphi\left(\sum_{j=1}^m \omega_{kj} x_j + b_k\right) \quad (3.1)$$

Or the bias b_k can be rewritten as $b_k = \omega_{k0} x_0$, then the equation 3.1 can be formulated as:

$$y_k = \varphi\left(\sum_{j=0}^m \omega_{kj} x_j + b_k\right) \quad (3.2)$$

Activation Function

The two most used activation functions are *threshold function* and *sigmoid function*.

The threshold function is as simple as:

$$\varphi(v) = \begin{cases} 1 & \text{if } v \geq 0 \\ 0 & \text{if } v < 0 \end{cases} \quad (3.3)$$

The sigmoid function is defined as:

$$\varphi(v) = \frac{1}{1 + \exp(-av)} \quad (3.4)$$

where a is the slope parameter of the sigmoid function. Different from equation 3.3, the equation 3.4 is differential, which is very important to a neural network. Hence, the sigmoid function is, in some way, more popular than threshold function.

3.1.2. Multilayer Feedforward Networks

Feedforward network is the first also important architecture. The information move direction is from input to output, without any recurrent loop. The structure of a simple multi-player feedforward network is shown in figure 3.2. In this example, the connections between nodes and layers are clearly stated. The information is first sent by source nodes in the input layer, through hidden layer(s), finally output by the last layer.

G.Cybenko proved, in 1989 that with sigmoid activation function, any given function can be represented by multi-player neural network[14]. Later in the year 1991, K. Hornik proved that any activation function can work too[22]. These are concluded as the *Universal Approximation Theorem* and it is stated as:

Under mild assumptions of the activation function, any continuous function on compact subsets of \mathbf{R}^n can be approximated by a feed-forward network with a single hidden layer.[57]

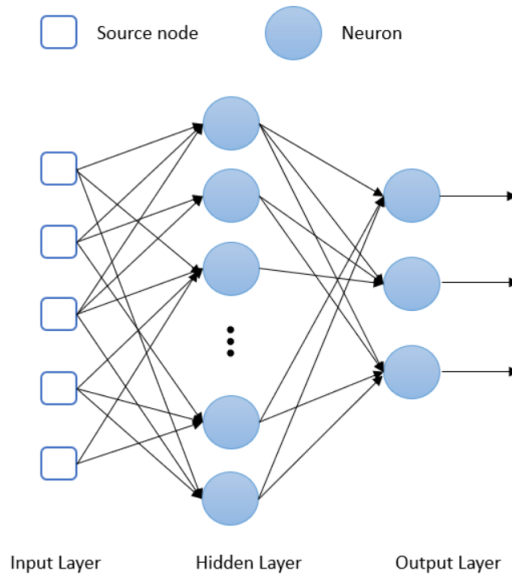


Figure 3.2: Multiplayer feedforward network with one hidden layer and one output layer

Of course, the number of hidden layers and their nodes can be adjusted in specific cases, instead of only one layer, to attain better learning results. However, the theorem doesn't touch upon the algorithm methods on the network parameters computation. For EM problem, it is not necessarily to have an ultra multiplayer network, since the design space of a particular antenna is limited to relatively small range compared to some more complicated learning cases, like image processing. Thus the network parameters in this thesis are more designed and optimized by experiments.

3.1.3. Backpropagation Algorithm

For multiplayer feedforward network, the learning techniques can be batch learning, on-line learning and backpropagation learning etc. Backpropagation somehow is the enhancement of on-line learning. In this thesis, the neural network will be constructed based on this algorithm for its maturity and high learning accuracy. Backpropagation algorithm[19] is a kind of supervised learning method in most of the cases. Here, the output error is computed by comparing the network outputs and the real training value and then the error is used as feedback to adjust the weights and layers of the network. The signal flow details of the kth neuron

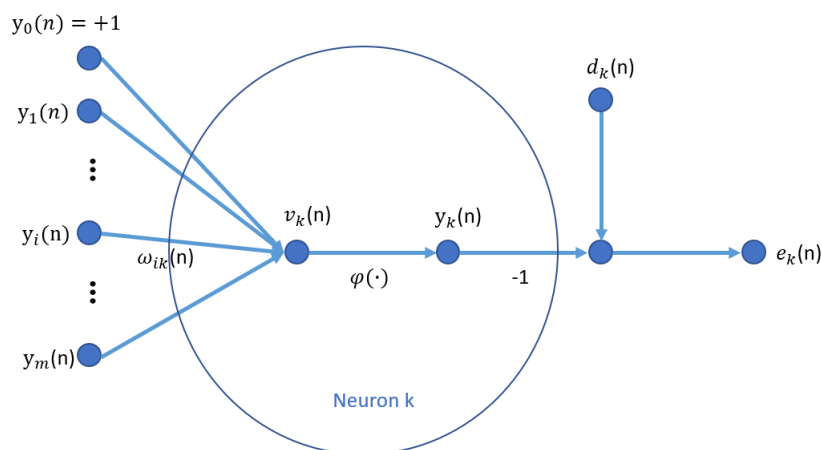


Figure 3.3: Signal flow of output neuron k

in the nth iteration are shown in figure 3.3. The outputs of neurons in the last layer function as the inputs of

neuron k. ω_{ik} is the weight of link between neuron i and neuron k. The local field v_k can be written as:

$$v_k(n) = \sum_{i=0}^m \omega_{ik}(n) y_i(n) \quad (3.5)$$

With the activation function $\varphi(\cdot)$, the output of neuron k is:

$$y_k(n) = \varphi(v_k(n)) \quad (3.6)$$

Comparing the output y_k with the target value d_k , the error can be computed as:

$$e_k(n) = d_k(n) - y_k(n) \quad (3.7)$$

According to the error e_k , the network will correct the weight ω_{ik} . Here the cost function, defined by Gauss-Newton method is introduced as:

$$\varepsilon(n) = \frac{1}{2} \sum_{k \in C} e_k^2(n) \quad (3.8)$$

By summing the $\varepsilon(n)$ of all the neurons in the output layer, the total instantaneous error energy of whole network $\varepsilon(n)$ is obtained. The weight correction is proportional to the partial derivation of $\varepsilon(n)$. Then by solving $\frac{\partial \varepsilon_k}{\partial \omega_{ik}}$, the correction $\Delta \omega_{ik}(n)$ can be found.

$$\frac{\partial \varepsilon_k}{\partial \omega_{ik}} = \frac{\partial \varepsilon(n)}{\partial e_k(n)} \frac{\partial e_k(n)}{\partial y_k(n)} \frac{\partial y_k(n)}{\partial v_k(n)} \frac{\partial v_k(n)}{\partial \omega_{ik}(n)} \quad (3.9)$$

Based on the chain rule of calculus, the Equation 3.9 can be resolved by differentiating both sides of the relative functions (equation 3.5–3.8) and the results are:

$$\frac{\partial \varepsilon(n)}{\partial e_k(n)} = e_k(n) \quad \frac{\partial e_k(n)}{\partial y_k(n)} = -1 \quad \frac{\partial y_k(n)}{\partial v_k(n)} = \varphi'(v_k(n)) \quad \frac{\partial v_k(n)}{\partial \omega_{ik}(n)} = y_i(n)$$

Then the equation 3.9 can be rewritten as:

$$\frac{\partial \varepsilon_k}{\partial \omega_{ik}} = -e_k(n) \varphi'(v_k(n)) y_i(n) \quad (3.10)$$

and the correction $\Delta \omega_{ik}(n)$ is:

$$\Delta \omega_{ik}(n) = -\eta \frac{\partial \varepsilon_k}{\partial \omega_{ik}} = \eta e_k(n) \varphi'(v_k(n)) y_i(n) \quad (3.11)$$

where η is the learning rate of the backpropagation algorithm. When η is small, the synaptic weight changes in small steps from one iteration to another, which means the changing process will be smoothly but the learning rate will be slow. On the other hand, if η is too big, learning process will definitely be faster, while the model will work under the risk of instability. To reduce the conflict between learning accuracy and speed, the generalized delta rule can be applied to function 3.11. The improved expression can be written as:

$$\Delta \omega_{ik}(n) = \alpha \Delta \omega_{ik}(n-1) + \eta \delta_k(n) y_i(n) \quad (3.12)$$

where $\delta_k(n) = e_k(n) \varphi'(v_k(n)) y_i(n)$ is the local gradient factor. α , normally positive, controls the feedback loop acting around $\Delta \omega_{ik}(n)$. The derive process can be found in [23].

The computation process above consists two phase of backpropagation algorithm. They are forward phase and backward phase. In the former part, the function signal y_k is computed and the synaptic weight remains unchanged for now. Then the function signal is compared with the target d_k and the error signal e_k can be found here. In a word, forward phase starts from the first hidden layer with passing the signal from input layer and ends at the output layer with the error signals. As for the backward phase, the error signal oppositely begin passing from the output layer and back toward the input layer, adjusting the synaptic weight based on the computation rule stated in function 3.11.

The adjustment of synaptic weight stops when the model attains some well-defined criterion. Here two convergence criterion, which are widely accepted, are introduced[29]:

1. "The backpropagation algorithm is considered to have converged when the Euclidean norm of the gradient vector reaches a sufficiently small gradient threshold."

However, for this criterion, the critical drawback is the longer training process and complicity in the computation of the gradient vector $g(\omega)$. Hence, another standard is provided as:

2. "The backpropagation algorithm converges when the absolute rate of change in the mean squared error per epoch is small enough.[19]"

The risk for the second criterion is that the error may be correlated for nonlinear models, even though the mean squared error or its variation rate is small[59]. To overcome this, more criterion is suggested in [4]. In a word, the forward pass and backward pass will be iterated by presenting new epochs of training samples to the network until it satisfies the prescribed stopping criterion.

3.1.4. Advantages of Neural Network

According to the definition mentioned in the beginning of the chapter, neural network has highly parallel computation structure and strong ability to learn from environment, thus neural network is regarded as a powerful method to be applied in pattern recognition and function fitting problems. Although it is still far away from constructing a neural network which can be comparable to human brain, it already shows many useful properties which are critical for complicated computation.

- **Nonlinearity:** Due to the nonlinear neurons that construct the interconnection, the nonlinearity is distributed all over the neural network. This enables the network to cope with the cases where the relationships between inputs and outcomes are highly nonlinear. For example, nonlinearity exists in most of the electromagnetic filed issues.
- **Input-Output mapping:** The supervised learning method[15], one of the most important learning methods in NN, can construct the input-output mapping of the target problems by learning from the a set of labeled training examples. This merit inspires the study of nonparametric statistical inference. "Nonparametric" suggests that there is no prior assumptions are made on a statistical model for the input data. In other word, the network, taught by a set of examples, can estimate arbitrary decision within the input signal space for the pattern-classification or function fitting problems.
- **Adaptivity:** As it is mentioned in last section, the synaptic weights of a neural network can be modulated in the training process, which means the NN is capable of adapting to the changes in the surrounding environment. It can even be designed to overwrite the weight value in real time when the NN is working in a non-stationary environment. Generally, when a system becomes more adaptive, the longer it can be stable, the more robustness can be achieved when the system is required to work in a changing environment[19]. However, this doesn't mean that adaptivity always brings in robustness. In [6], the dilemma between adaptivity and robustness, as well the relative solutions, are introduced.
- **Fault Tolerance:** A neural network, in some extent, can be regarded as fault tolerant. This is due to the distributivity of the information on the whole neural network. When part of the neurons and their connections crash, as long as they are not extremely extensive, the performance of the neural network will degrade in a graceful way. In practical, measurements in algorithm designing process can be taken to ensure the fault tolerance of the NN in a better way.

Neural network is advantageous in many other aspects either. For example, the highly parallel structure of NNs provides fast computation speed for specific tasks. Also, it makes the possibility to implement vary-large-scale-integrated (VLSI) technology for the NNs, which means there is a chance for NNs to extract very complex behavior in the highly hierarchical issues.

These merits of neural network are strong reasons for its application in electromagnetic related problems, considering that the analysis of EM filed is mostly underlying complicated nonlinear environment and requires for large amount of computation. In the later chapters, the thesis will specify how to implement the neural network on assessing the performance of a dielectric resonant antenna when different antenna parameters are given.

3.2. Support Vector Machine

Support vector machine(SVM), an elegant kernel-learning method, is another important machine learning algorithm. The main idea of SVM is:

"The support vector machine can construct a hyperplane as a decision surface under a given training sample. The margin of separation between positive and negative examples is maximized[19]."

Based on this concept, SVM is developed to deal with the more difficult case of nonlinearly separable pattern. However, at the very beginning, the SVM can be simply described by a classical binary classification problem.

3.2.1. Linearly Separable Patterns

Spots with two different colors are shown in figure 3.4 (a). Surface A and B are used to divide these spots into two groups by colors. These surfaces are called "decision surface" in SVM. The positions of the dotted lines are decided by the orientation of the decision surface and the spots which are the nearest to the surface. The area between the two dotted lines is the "margin of separation". Referring to the idea of SVM, decision surface A is thought to be better than B, since the margin of separation is obviously wider in (b). If the margin of separation in (b) is the maximum one that can be found, then the decision surface A is called the "optimal hyperplane". In a word, the task of SVM is to find the optimal hyperplane.

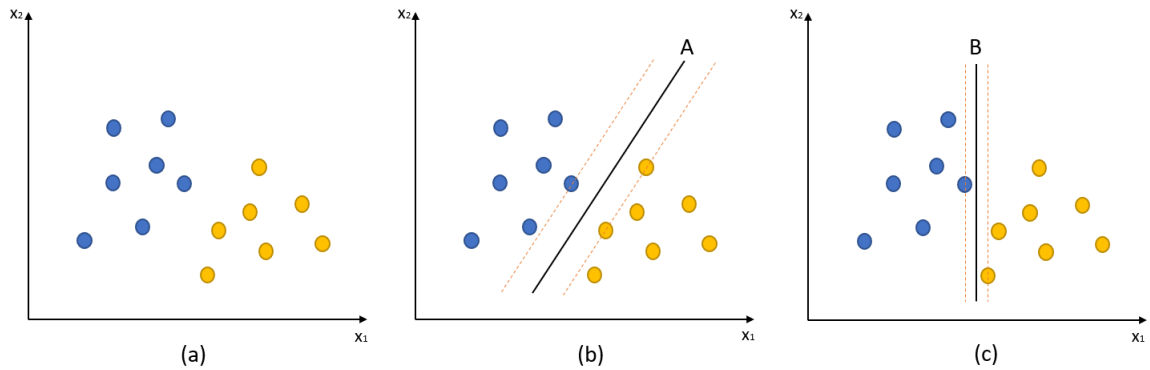


Figure 3.4: Description for binary classification problem (adopted from [10]): (a) Two different groups of spots; (b) Divide spots by hyperplane A; (c) Divide spots by hyperplane B

The surface plane can be expressed as:

$$\boldsymbol{\omega}^T \mathbf{x} + \gamma = 0 \quad (3.13)$$

The bold symbols represent vectors. So $\boldsymbol{\omega} = [\omega_1, \omega_2]^T$ is the weight vector and $\mathbf{x} = [x_1, x_2]^T$ is an input vector. γ is the bias. The size of the separation margin can be simplified as the computation of distance "d", shown in figure 3.5, from the closest spots to the decision surface. d can be computed as[1]:

$$d = \frac{|\boldsymbol{\omega}^T \mathbf{x} + \gamma|}{\|\boldsymbol{\omega}\|} \quad (3.14)$$

Now the objective function 3.14 is obtained. Another critical factor for classification problem is the constraint condition. For this linearly separation problem, there are three constraint conditions:

1. The plane should divide all the spots into the right group;
2. Bias γ should make the decision surface in the middle of the margin of separation;
3. The vector \mathbf{x} in the objective function should be the support vector, which means the points in \mathbf{x} should be the samples that are closest to the decision surface.

In order to express the constraint conditions, each sample point x_i is labeled as y_i , meaning:

$$y_i = \begin{cases} +1 & \text{for } \textit{yellow points} \\ -1 & \text{for } \textit{blue points} \end{cases} \quad (3.15)$$

Then the first constraint condition can be expressed as:

$$\begin{cases} \boldsymbol{\omega}^T \mathbf{x}_i + \gamma > 0 & \text{for } y_i = +1 \\ \boldsymbol{\omega}^T \mathbf{x}_i + \gamma < 0 & \text{for } y_i = -1 \end{cases} \quad (3.16)$$

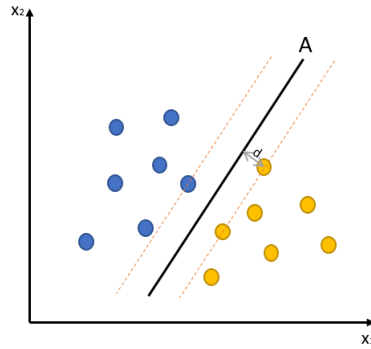


Figure 3.5: Computation of the separation margin(adopted from [10])

The second constraint condition can be written as:

$$\begin{cases} (\boldsymbol{\omega}^T \mathbf{x}_i + \gamma) / \|\boldsymbol{\omega}\| \geq d & \forall y_i = +1 \\ (\boldsymbol{\omega}^T \mathbf{x}_i + \gamma) / \|\boldsymbol{\omega}\| \leq -d & \forall y_i = -1 \end{cases} \quad (3.17)$$

If both sides of equation 3.17 are divided by d, a new group of equations can be attained:

$$\begin{cases} (\boldsymbol{\omega}_d^T \mathbf{x}_i + \gamma_d) \geq 1 & \forall y_i = +1 \\ (\boldsymbol{\omega}_d^T \mathbf{x}_i + \gamma_d) \leq -1 & \forall y_i = -1 \end{cases} \quad (3.18)$$

where

$$\boldsymbol{\omega}_d = \frac{\boldsymbol{\omega}}{\|\boldsymbol{\omega}\|d}, \quad \gamma_d = \frac{\gamma}{\|\boldsymbol{\omega}\|d}$$

Since $\|\boldsymbol{\omega}\|d$ is a constant for one surface, then the equation 3.18 can be simplified as:

$$\begin{cases} (\boldsymbol{\omega}^T \mathbf{x}_i + \gamma) \geq 1 & \text{for } y_i = +1 \\ (\boldsymbol{\omega}^T \mathbf{x}_i + \gamma) \leq -1 & \text{for } y_i = -1 \end{cases} \quad (3.19)$$

Now the function 3.19 can be regarded as the fundamental description of the constraint conditions for SVM optimization problem. When x_i is the sample of support vector, the equation can establish. Combine with the equation 3.14, the distance between the support vector sample and the decision surface can be written as:

$$d = \frac{|\boldsymbol{\omega}^T \mathbf{x}_i + \gamma|}{\|\boldsymbol{\omega}\|} = \frac{1}{\|\boldsymbol{\omega}\|} \quad (3.20)$$

where x_i is a support vector.

Like what is mentioned before, the task of SVM is to find the proper parameters $(\boldsymbol{\omega}, \gamma)$ to make the margin of separation, $W = 2d$, reach the maximum. In other words, the problem is transferred to minimize $\|\boldsymbol{\omega}\|$, amounting to the minimization $\frac{1}{2}\|\boldsymbol{\omega}\|^2$. The coefficient $\frac{1}{2}$ and squaring are applied only for simplifying the later derivation process.

The mathematic description of the SVM optimization problem for the linearly separation pattern can be concluded as:

$$\begin{aligned} & \min_{\boldsymbol{\omega}, \gamma} \frac{\|\boldsymbol{\omega}\|^2}{2} \\ & \text{s.t. } y_i(\boldsymbol{\omega}^T \mathbf{x}_i + \gamma) \geq 1, \quad i = 1, 2, \dots, m \end{aligned} \quad (3.21)$$

3.2.2. Non-separable Pattern

In practice, however, things become more complicated. Like what is shown in figure 3.6 (a), there are two "irregular" points which result these points cannot be divided by a single line or plane anymore. Another situation is shown in (b), the model can still be divided, but the generalization ability of the decision surface

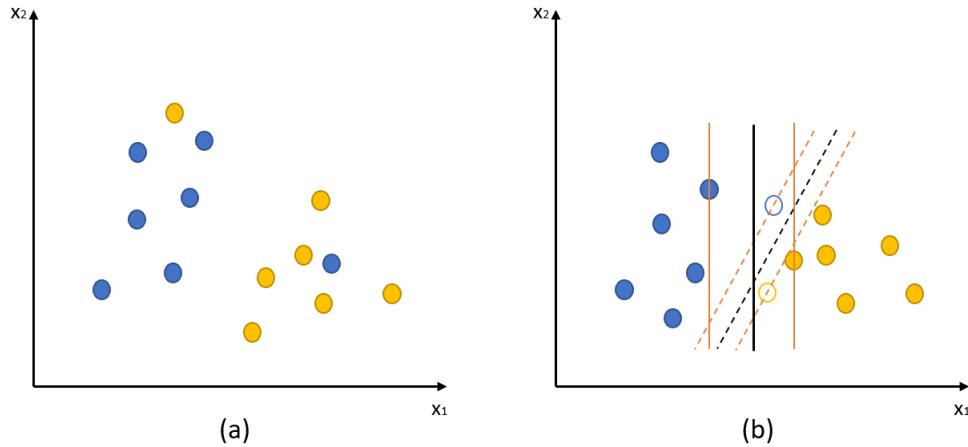


Figure 3.6: Non-separable Patterns

is weakened seriously by the two "irregular" points.

Due to these problems, the soft separation margin is introduced. Compared to the hard margin of separation 3.21, a slack variable is lead-in. Correspondingly, the slack variables will result in extra costs. Hence, the learning conditions of SVM for soft margin are rewritten as[3]:

$$\begin{aligned} \min_{\omega, \gamma} \frac{1}{2} \|\omega\|^2 + C \sum_{i=1}^m \xi_i \\ \text{s.t. } y_i(\omega^T \mathbf{x}_i + \gamma) \geq 1 - \xi_i, \quad i = 1, 2, \dots, m \\ \xi_i \geq 0, \quad i = 1, 2, \dots, m \end{aligned} \quad (3.22)$$

Where ξ_i is the slack variant and C is the penalty factor. With ξ_i , the distances between the support vectors and the decision surfaces are no longer strictly required to be bigger than 1. The penalty factor C is used to control the influence of the error. The bigger the C is, the greater penalty for misclassification and vice versa. In practice, C will be selected through parameter adjusting. Functions 3.22 can be optimized and solved based on Lagrange function. The details can be found in [17], which are not recorded here.

3.2.3. Kernel Functions for SVM

Above the hard separation margin and the soft margin are discussed. They are very useful on dealing with the linearly separable patterns. However, SVM becomes weak when the pattern is not linearly separable anymore. The problem motivates people to map the data into a possibly higher dimensional vector space where the linear relationship stands again. Then a linear algorithm can be applied in this new space. However, another problem cropped up. Representing data into high dimensional space, sometimes when the mapping dimension is too high, is computationally difficult. That's why an alternative solution, kernel function, is put forward[5].

Kernel function, in short, is used to calculate a similarity measure in the feature space instead of the coordinates of the vectors there. Then apply algorithms that only need the value of this measure[32]. The similarity measure is a dot product. More formally, kernel function can be defined as:

Suppose ϕ is a H-mapping from a low-dimensional input space χ to a high-dimensional Hilbert space. If there is a function $\kappa(\mathbf{x}, \mathbf{z})$, for any $\mathbf{x}, \mathbf{z} \in \chi$, there is:

$$\kappa(\mathbf{x}, \mathbf{z}) = \langle \phi(\mathbf{x}) \cdot \phi(\mathbf{z}) \rangle$$

where bold letters \mathbf{x}, \mathbf{z} represent vectors and $\langle \cdot \rangle$ means inner production. Then $\kappa(\mathbf{x}, \mathbf{z})$ is called **Kernel Function**. With kernel function, computation in high dimensional space is avoided, since $\kappa(\mathbf{x}, \mathbf{z})$ is computed in the low dimensional feature space and the classification results are actually mapped to the high dimensional space.

Here, the most popular kernel functions are concluded[8]:

1. **Linear Kernel:** The function that is used in linearly separable SVM

$$\kappa(\mathbf{x}, \mathbf{z}) = \mathbf{x} \cdot \mathbf{z}$$

2. **Polynomial Kernel:** Common kernel that is used in linearly non-separable SVM

$$\kappa(\mathbf{x}, \mathbf{z}) = (\gamma \mathbf{x} \cdot \mathbf{z} + r)^d$$

where parameters γ, r, d are needed to be optimized through experiments and d means degree of polynomial equation.

3. **Gaussian Kernel:** This is also called *Radial Basis Function, RBF*. It is the most popular kernel function for nonlinear classification and regression in SVM field.

$$\kappa(\mathbf{x}, \mathbf{z}) = \exp(-\gamma \|\mathbf{x} - \mathbf{z}\|^2 + r)$$

where $\gamma > 0$

4. **Sigmoid Kernel:** Another common function for linearly non-separable SVM

$$\kappa(\mathbf{x}, \mathbf{z}) = \tanh(\gamma \mathbf{x} \cdot \mathbf{z} + r)$$

3.2.4. Support Vector Regression

In above sections, the utilization of support vector on classification and relative algorithms have been introduced. In fact, SVM can also be applied to solve regression problems, such as function fitting and pattern recognition. This is one reason that SVM is thought to be promising in this project.

Unlike the classification model, the object for regression is to make each point in the training dataset can be as close as possible to a linear model. Usually, the mean square error is regarded as the loss function for regression model. However, for support vector regression problem, the loss function is defined[38] as:

$$err(x_i, y_i) = \begin{cases} 0 & \text{for } |y_i - \omega \cdot \phi(x_i) - b| \leq \epsilon \\ |y_i - \omega \cdot \phi(x_i) - b| - \epsilon & \text{for } |y_i - \omega \cdot \phi(x_i) - b| > \epsilon \end{cases} \quad (3.23)$$

ϵ is a predefined constant, which is always bigger than 0. For any point (x_i, y_i) , if $|y_i - \omega \cdot \phi(x_i) - b| \leq \epsilon$, then it is thought to be fit the pattern or function well. In other word, this point locates in the acceptable area which is shown in figure 3.7 with yellow color. Otherwise, the loss is brought in and the loss can be expressed by the length of the red line. Thus, the regression model of SVM can be concluded as 3.24:

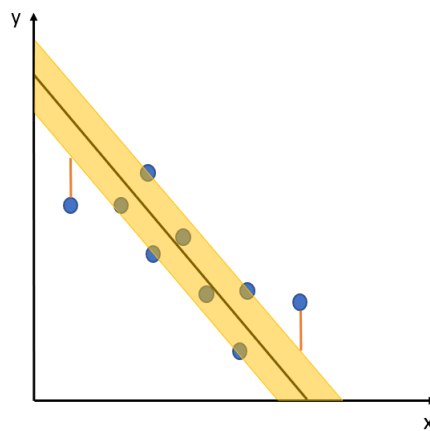


Figure 3.7: Description for linear regression problem of SVM (adopted from [10])

$$\begin{aligned}
& \min \quad \frac{1}{2} \|\omega\|^2 + C \sum_{i=1}^m (\xi_i^V + \xi_i^\wedge) \\
& \text{s.t.} \quad -\epsilon - \xi_i^V \leq -\omega \cdot \phi(x_i) - b \leq \epsilon + \xi_i^\wedge \quad i = 1, 2, \dots, m \\
& \quad \quad \xi_i^V \geq 0, \quad \xi_i^\wedge \geq 0 \quad i = 1, 2, \dots, m
\end{aligned} \tag{3.24}$$

where ξ_i^V and ξ_i^\wedge both are slack variant. The computation process of solving the function 3.24 can be found in many classical literatures, such as [19], which will not be repeat here.

3.3. Conclusion

In this chapter, two proposed machine learning methods, neural network and support vector machine, have been discussed. For neural network, the author mainly study about the multilayer feedforward network that is trained by backpropagation algorithm. For SVM, the principles of dealing with the classification and regression problems are learned.

In a word, both of NN and SVM show their potential to model and assess the rectangular DRA in this thesis. Hence, the decision that which method will be finally applied in this thesis can be made only after comparing their ability of predicting the RDRA's performance.

4

Learning Model for the RDRA Design

Purpose of this chapter is to construct the proper learning models for the rectangular dielectric resonant antennas. There is no possibility for a learning model to predict the antennas' performance indefinitely, so the design space of a rectangular DRA is firstly specified in this chapter. This space is required to compromise the theories of RDRA, also the practical application. An amount of training and test data will be simulated within this design space. Later, two training models, neural network model and SVM model, will be built by applying the training data. Their training results will be tested by data which is out of the training dataset. The better learning model will be chosen through comparison. The last step is about optimizing the model.

4.1. Design Space of Rectangular DRA

4.1.1. Definitions of Antenna Parameters

The performance of an antenna can be characterized in several different ways. This section will introduce some fundamental parameters of antennas[12]. The learning model which will be designed in this project is to predict parts of these parameters. In other words, the learning model can predict the antenna performance in some way by estimating these parameters.

Radiation Pattern

According to the *IEEE Standard Definitions of Terms for Antennas (IEEE Std 145-1983)*, antenna radiation pattern is defined as "**a mathematical function or a graphical representation of the radiation properties of the antenna as a function of space coordinates. In most cases, the radiation pattern is determined in the far field region and is represented as a function of the directional coordinates.**"

A single power pattern of an antenna array is shown in figure 4.1. The antenna radiation power is normalized to their maximum value. Normally, the power pattern is plotted on a logarithmic scale and the unit is "dB", since the logarithmic scale can contain more details for those parts where the power is too small or very large. "Lobes" describe different parts of the pattern, which may be subclassified into main and minor lobes. Main lobe is "the radiation lobe containing the direction of maximum radiation. (*IEEE Standard Definition*)" For some antennas, there may be more than one main lobe. On the other hand, minor lobes represent any lobes except the main lobe, including side lobe and back lobe, which are usually the power radiation in the undesired directions.

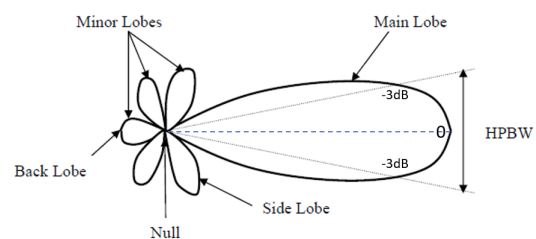


Figure 4.1: Two-dimensional normalized power pattern (in dB, adopted from [47])

Beamwidth

Beamwidth is another parameter which is associated with the radiation pattern. It is the "**angular separation between two identical points on opposite side of the pattern maximum[12]**". In figure 4.1, "HPBW" represents one of the most used beamwidth - the *Half-Power Beamwidth*. HPBW, defined by IEEE, is the angle,

in the plane containing the directions of the maximum of a beam, between the two directions in which the radiation intensity is one-half value of the beam. In power radiation pattern, HPBW means the angle of the area which is within the two "-3dB" points, as it is shown in figure 4.1. In practice, if no specific notification, the term *beamwidth* refers to HPBW.

Beamwidth is an important index since it can be used as the trade-off of main lobe and minor lobes. With beamwidth increases, the level of the side lobes will decrease. In other words, more energy will be radiated in the desired direction when beamwidth is comparably wide. In this project, beamwidth is a estimated object of the learning model.

Directivity

In the 1993 version of the *IEEE Standard Definition of Terms for Antennas*, directivity of an antenna is defined as "**The ratio of the radiation intensity in a given direction from the antenna to the radiation intensity averaged over all directions**". The average radiation intensity equals to the total antenna radiation power divided by 4π . If no specific direction is provided, the direction of maximum radiation intensity is implied. In mathematical form, directivity is written as:

$$D = \frac{U}{U_0} = \frac{4\pi U}{P_{rad}} \quad (4.1)$$

where U is the radiation intensity and U_0 is the radiation intensity of isotropic source.

In this project, the antenna radiation pattern is directional since the dielectric resonator can somehow guide the power radiated from the feedline. For directional pattern, the computation of directivity can be approximated as[12]:

$$D_0 = \frac{4\pi}{\Omega_A} \approx \frac{4\pi}{\theta_{1r}\theta_{2r}} \quad (4.2)$$

The Ω_A is the beam solid angle of radiation pattern and it is close to the product of θ_{1r}, θ_{2r} , where θ_{1r} and θ_{2r} , shown in figure 4.2, are the HPBW in two planes which are mutually orthogonal. Unit of these two HPBWs are all in radians.

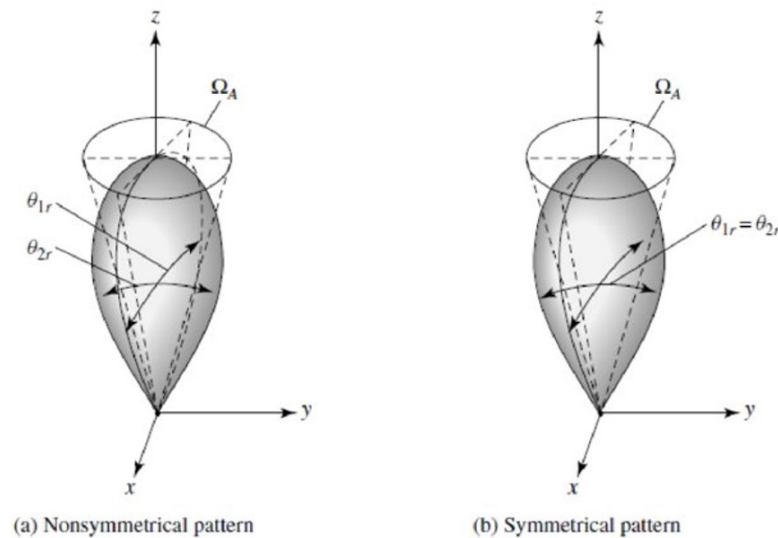


Figure 4.2: Antenna directivity calculation by antenna beam solid angles[12]

Antenna Efficiency

Not all the power transferred to the antenna can be radiated. Part will be lost due to the reflection caused by the mismatch between the feeding transmission line and the antenna. The conduction and dielectric losses also lead to decreasing antenna efficiency. Generally, the efficiency of antenna can be computed as[12]:

$$e_0 = e_r e_c e_d \quad (4.3)$$

where:

e_0 is the total efficiency;

e_r is the mismatch efficiency. $e_r = (1 - |\Gamma|^2)$;

Γ is voltage reflection coefficient at the input terminals of an antenna and it can be written as:

$$\Gamma = \frac{Z_{in} - Z_0}{Z_{in} + Z_0} \quad (4.4)$$

Z_{in} is the antenna input impedance which will be introduced later. Z_0 is characteristic impedance of the transmission line;

e_c is conduction efficiency;

e_d is dielectric efficiency.

e_c and e_d are usually determined by experiments instead of computation which is quite difficult. What needs to be noticed is that the experimental measurements for e_c and e_d are always combined. Hence, the equation 4.3 is usually rewritten as:

$$e_0 = e_{cd}e_r = e_{cd}(1 - |\Gamma|^2) \quad (4.5)$$

where e_{cd} implies antenna radiation efficiency.

From function 4.5, it is clear that the antenna efficiency is tightly related to the reflection factor. Under the same radiation efficiency, the smaller is the Γ , the higher antenna efficiency is. Whether in the process of theoretical design, or based on the requirements of industrial products, this index is very important. Thus, in this project, the reflection factor is selected as one of the learning objects for the model.

Gain

Gain is another parameter of antenna performance which is close to directivity, but gain contains the influence of antenna efficiency and its directional ability. According to the IEEE definition, gain is "*the ratio of the intensity to the radiation intensity that would be obtained if the power accepted by the antenna were radiated isotropically in a given direction.*" The mathematical expression of gain is:

$$Gain = 4\pi \frac{U(\theta, \phi)}{P_{in}} \quad (4.6)$$

where

$U(\theta, \phi)$ is the radiation intensity;

P_{in} is the total input power that the antenna received. Since there is the relationship that $P_{rad} = e_{cd}P_{in}$, the equation 4.6 can be written as:

$$G(\theta, \phi) = e_{cd} \left[4\pi \frac{U(\theta, \phi)}{P_{rad}} \right] \quad (4.7)$$

Combined with equation 4.1, the relationship between antenna gain and directivity can be found:

$$G(\theta, \phi) = e_{cd}D(\theta, \phi) \quad (4.8)$$

Input Impedance

Input impedance is "*the impedance presented by an antenna at its terminals*". Antenna input impedance is crucial to the power radiated and received by the antenna. Here, take the transmit mode of antenna as an example. Its Thevenin equivalent circuit is shown below. According to the circuit 4.3, the antenna resistant can be written as:

$$R_A = R_r + R_L \quad (\Omega) \quad (4.9)$$

where R_r is the antenna radiation resistant and R_L is the loss resistance of antenna.

Consider the antenna reactance, the input impedance is:

$$Z_A = R_A + jX_A \quad (\Omega) \quad (4.10)$$

The left side at the terminal a-b (in figure 4.3) is a generator, whose impedance is:

$$Z_g = R_g + jX_g \quad (\Omega) \quad (4.11)$$

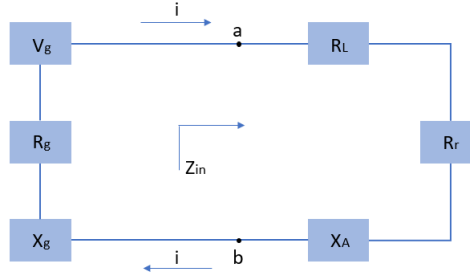


Figure 4.3: Thevenin equivalent circuit of antenna transfer mode[12]

where R_g and X_g are the resistance and reactance of the generator respectively. The circuit current i (unit: Ampere) can be computed now.

$$i = \frac{V_g}{Z_A + Z_g} = \frac{V_g}{(R_r + R_L + R_A) + j(X_A + X_g)} \quad (A) \quad (4.12)$$

where the V_g is the peak voltage of the generator. The power (unit: Watt) radiated by the antenna radiation resistant R_r can be obtained;

$$P_r = \frac{1}{2} |I_g|^2 R_r = \frac{1}{2} |V_g|^2 \left[\frac{R_r}{(R_A + R_g)^2 + (X_A + X_g)^2} \right] \quad (W) \quad (4.13)$$

The maximum radiated power is achieved when $R_A = R_g$ and $X_A = -X_g$. The maximum radiated power is:

$$P_r = \frac{1}{2} |V_g|^2 \left[\frac{R_r}{(2R_A)^2} \right] = \frac{1}{8} |V_g|^2 \left[\frac{R_r}{(R_r + R_L)^2} \right] \quad (W) \quad (4.14)$$

In practice, it is important to match the antenna impedance to the connected circuit so that the most of the power can be radiated. In order to realize this, a matching circuit may be inserted between generator and the antenna. Knowing the input impedance is crucial during the design process of the antenna. Hence, in this project, the learning model will also be trained to calculate the antenna input impedance.

A short summary

Some of the antenna parameters were introduced briefly in this section. They were the antenna radiation pattern, beamwidth, directivity, antenna efficiency, gain and input impedance. Among these parameters, the HPBW, reflection factor and input impedance were chosen as the learning objects of the learning model.

4.1.2. Practical Requirements on Antenna Parameters setting

In Chapter 2, the advantages of the rectangular dielectric resonant antenna have been stated, as well as some design principles and theories. The performance of the RDRA is difficult to be analyzed by classical numerical method. The purpose of this project, to emphasis again, is to construct a learning model which is capable of predicting the antenna performance under some preset parameters. A design space should be defined beforehand, so that the model can be more objective.

Slot aperture feed method

In figure 4.4, the sketch of the aimed RDRA is shown. The resonant cube is on the top of the ground plane, where the slot aperture is. Under the plane is the substrate board. The feed line is attached below the substrate. The signal of 24 GHz will be input from the end of the feed line. Reason to choose this topology is stated in the *Internship Progress Report* of the writer, which will not be repeat here.

Since the working frequency is asked to be 24 GHz, the slot length is supposed to be around the half of the wavelength (refer in Chapter 2).

$$L_{slot} \approx \frac{1}{2} \lambda_0 = \frac{1}{2} \times \frac{c}{f_0} = \frac{1}{2} \frac{3 \times 10^8}{24 \times 10^9} = 0.00625 \quad (m)$$

where c is the light speed in vacuum.

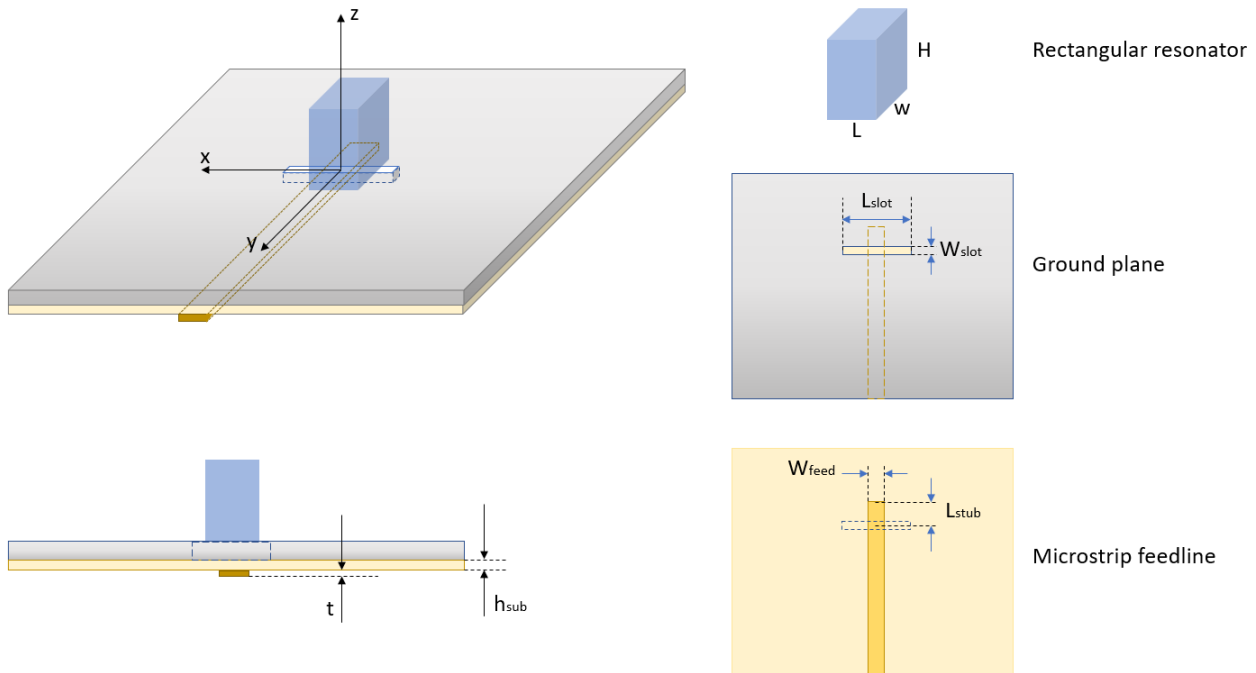


Figure 4.4: Schematic diagram of rectangular DRA structure

Consider the error and manufacture accuracy, the slot length is made as 6.3 millimeter in this project. The slot width, W_{slot} , should be as small as possible. In practical design, the value of W_{slot} is usually one tenth of the slot length. Too narrow a slot makes it difficult and expensive to manufacture. Hence, in this project, $W_{slot} = 0.63$ millimeter. The ground plane is made of aluminum, which is a good conductor and relatively cheap. The thickness of the ground plane is 1 millimeter. Under the aluminum board is the substrate layer. The material of this layer is Rogers 4350B, whose relative dielectric constant is 3.48 at 24 GHz[13]. The height of the substrate, h_{sub} is 0.508 mm. The lowest part is a microstrip feedline that is made of the copper. Generally, the thickness of copper microstrip, t , is as thin as 0.035 mm in industry. Width of the feedline, W_{feed} , can be computed according to the equation[7] below:

$$W_{feed} = \frac{7.48 \times h_{sub}}{e^{(z_0 \frac{\sqrt{\epsilon_r + 1.41}}{87})}} - 1.25 \times t \quad (m)$$

where ϵ_r is the relative dielectric constant of the substrate, equal to 3.48 here. The computed result of W_{feed} is around 1.02 mm. However, through simulation on the port impedance, the value is adjusted to 1.05 mm.

As for the L_{stub} , it represents how long the feedline exceeds the center of the slot. In theory, the microstrip stub can be open-circuited or short-circuited. For ease of fabrication the former is selected. As discussed in Chapter 2, L_{stub} is crucial to the coupling between the feedline and the slot aperture. Normally, in order to excite the aperture efficiently, the length of the stub should be around one fourth of the wavelength which is transmitted on the feedline. However, a center-fed slot antenna in this way has a very big radiation resistance which is around 300 Ohm. In [2], the stop tuning method is introduced. Adjusting the stub length can lead to an extra reactive loading on the antenna which can change the resonant frequency. In other words, L_{stub} should vary with different materials of substrate layer and the resonant cube which can influence the antenna impedance. For this reason, L_{stub} is regarded as an input feature of the learning model. Its range of variation should be from slightly less than 1/4 wavelength to slightly larger than 1/2 wavelength. So the learning area of L_{stub} is from 2 mm to 7 mm.

Ground plane

Also in Chapter 2, the influence of a finite ground plane was shortly discussed. In different literature, various methods are used to analyze how the size of the ground plane affects the antenna radiation. But the same

problem for the analysis on the ground plane size is the computation complexity. Hence, the dimensions of the ground plane are also taken into the learning feature space. The setting of ground plane is shown in figure 4.5. Taking the slot center as the origin point, four directions are defined. They are the positive direction and negative directions on both X axis and Y axis, labeled with dx_p , dx_n , dy_p and dy_n respectively.

The maximum values of these four factors are set as 25 mm, which is two times of the free-space wavelength λ_0 . In other words, the maximum ground plane is 50 mm \times 50 mm. The minimum distance between the slot center and the board edge is set as, 6.25 mm, the half wavelength of the transmitted wave.

Rectangular resonator

The last part is the dielectric resonator cube. As shown in figure 4.4, the cube edge that is along X axis is called length, labeled with "L". The edge that is perpendicular to the ground plane is the height, labeled with "H". The last edge of the cube is defined as the width, labeled with "W". These three dimensions of the resonator decide wave mode that is transmitted in it. Also, they affect the resonant frequency and antenna input impedance together. Hence, **H**, **L**, **W** are all regarded as the input features of the learning model. Consider that too small sizes will cause trouble for cube fabrication and too large sizes will result in higher modes transmitted in the resonator. The learning range for each dimension is set between 3 mm and 10 mm.

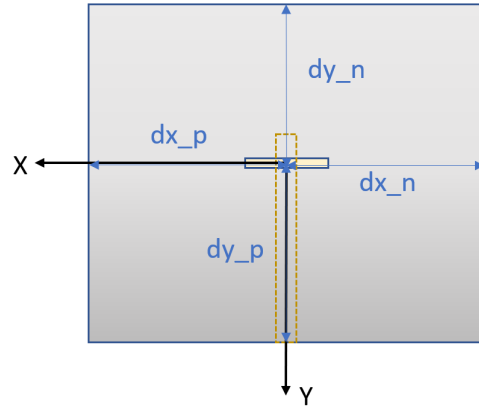


Figure 4.5: Dimensions of the antenna ground plane

Except the cube dimensions, the relative dielectric constant ϵ_r of the resonator is also vital. In this project, the resonator uses uniform material, hence ϵ_r of the cube should be a constant. In [40], several materials are provided. The common used materials for the transparent DRA are polycarbonate, K9 glass and so on. ϵ_r of these materials varies from 2 to 6. That's why the learning range of the relative dielectric constant of the resonator is set as 2 to 6.

What should be noticed again is that the rectangular resonator is placed at the center of the slot and one of the cube edges (length) is parallel to the slot.

A short summary

Now all the antenna parameters that will be taken as the input features of the learning model are specified. They are the three dimensions and dielectric constant of the resonator (H, L, W, ϵ_r), distances from the slot center to board edges in four directions (dx_n, dy_n, dx_p, dy_p) and the feedline stub length (L_{stub}). There are nine features in total (shown in table 4.1).

Learning feature	Dimension of resonator				L2 board(groundplane)				Feedline
	H	L	W	ϵ_r	dx_n	dy_n	dx_p	dy_p	L_{stub}
Learning range	3 mm to 10 mm			2 to 6	6.25 mm to 25 mm				2 mm to 7 mm

Table 4.1: Input features setting of the learning model

4.1.3. The Collection and Classification of Data

An effective dataset is compulsory for training and testing the learning model, no matter whether the SVM or neural network is used. In order to have this dataset, antenna models are simulated by using software *CST STUDIO SUITE* version 2018. For the purpose of saving time, the entire antenna is fed by a waveguide port in the simulation. In figure 4.6, an example of simulation model is given. The setting of the waveguide port area can make the port impedance is 50.56 Ohm, which is very close to 50 Ohm.

By sweeping the antenna parameters, a dataset with 3161 samples are finally obtained. The step size of each feature is randomly taken during the simulation. Among all the data, a group of testing data should be separated for model test after training has occurred. The test group is also supposed to be selected randomly. However, since for the usable antenna, there are some requirements on its performance. Like what is introduced in the former section of this chapter, the learning objects in this project are the reflection factor, antenna input impedance and 3dB angular beamwidth. For these three indexes, the interested ranges are set here:

1. Reflection factor: $S_{11} < -15$ dB;
2. Input impedance: $40 < R_A < 60$ Ohm; $-20 < X_A < 20$ Ohm
where R_A is the resistance of the input impedance, while X_A is the reactance;
3. 3dB angular beamwidth: $HPBW > 60$ degree

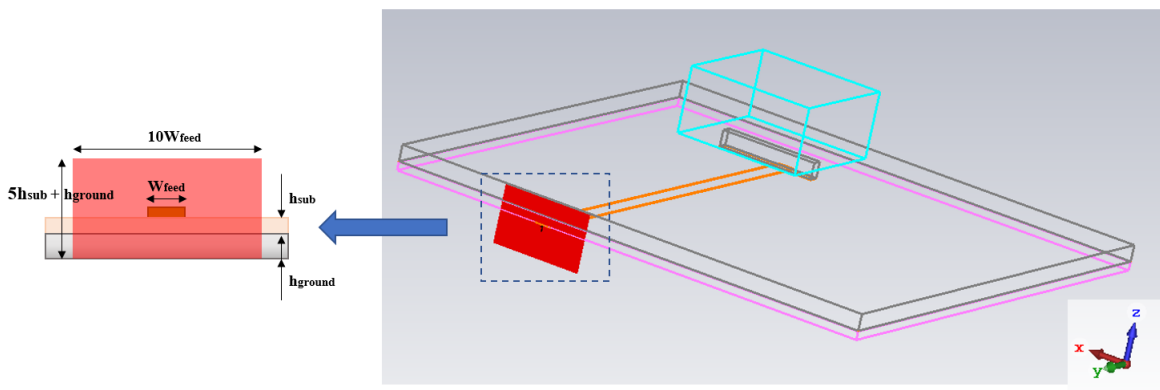


Figure 4.6: Simulation model and its waveguide port of RDRA (Construct on CST microwave studio 2018)

According to the interested ranges, 15 sets of data for each learning object, 60 sets in total, are picked from the whole dataset to make up the test data group. Table 4.2 shows all the test data that is selected. It is clear that the test data is intentionally chosen for every 15 sets though, the whole dataset is still evenly distributed. Now the dataset, excluded the test data, can be used for model training process, which means that there are 3101 samples in total that can be used to teach the model.

4.2. Construction of the Training Model

In this section, the process about how to build a neural network and a support vector regression machine will be illustrated, as well the model parameters. Following paragraphs start with neural network construction and then is the SVM.

4.2.1. Requirements of the Learning Model

Before constructing the models, some requirements are set for the final outcomes. By applying the test dataset to the trained models, the mean error between the learning outcomes and simulation data can be computed:

$$mean\ error = \frac{1}{N} \sum_{i=1}^N \|x_i - \bar{x}_i\|$$

where N is the amount of test data sets, x_i is the i th set of test data and \bar{x}_i is the learning result of the i th test data set. For the models, they are required to attain the objections below:

1. For reflection factor: $Mean\ error_{s_{11}} < 3$ dB
2. For resistance of antenna: $Mean\ error_{R_{in}} < 5$ Ω
3. For reactance of antenna: $Mean\ error_{X_{in}} < 10$ Ω
4. For 3dB angular width of antenna: $Mean\ error_{HPBW} < 10^\circ$

No.	1	2	3	4	5	6	7	8	9	10	11	12	13	14	15
S11	-25.81	-16.71	-18.33	-33.03	-20.8	-18.29	-29.45	-23.84	-17.82	-19.5	-35.48	-16.88	-15.19	-16.13	-19.7
RA	52.56	55.899	43.805	48.947	53.89	63.228	47.765	50.798	39.8	62.543	49.524	49.545	72.578	59.536	45.399
XA	5.106	-15.02	8.9594	0.6292	9.1941	-6.868	-0.182	-6.556	3.0139	-3.721	-0.652	14.472	1.0892	15.229	8.2514
HPBW	51.551	48.682	96.619	89.054	48.749	76.086	85.507	70.009	101.36	72.158	87.254	88.077	86.207	65.236	69.036

(a)

No.	16	17	18	19	20	21	22	23	24	25	26	27	28	29	30
S11	-8.571	-6.962	-8.548	-2.905	-13.49	-9.209	-13.23	-13.1	-4.058	-14.21	-5.352	-10.44	-9.44	-10.98	-7.29
RA	53.946	49.431	46.627	40.794	40.359	48.629	49.434	44.196	41.587	56.152	51.089	40.136	55.414	47.264	58.831
XA	42.085	50.412	39.083	-92.99	-16.5	-36.73	22.397	-20.43	73.542	-20.65	-65.56	-26.34	37.884	28.691	51.951
HPBW	75.486	59.048	110.48	44.189	68.035	63.445	54.642	71.167	85.657	100.64	50.888	51.793	83.316	71.007	86.608

(b)

No.	31	32	33	34	35	36	37	38	39	40	41	42	43	44	45
S11	-12.46	-4.58	-9.614	-11.64	-11.05	-10.01	-6.586	-7.454	-5.133	-3.609	-2.229	-6.146	-14.76	-10.06	-10.01
RA	38.513	13.168	27.237	79.697	31.764	93.691	139.18	20.807	14.728	10.476	6.5653	18.991	37.681	26.939	97.865
XA	-17.74	0.0062	10.677	-19.52	13.391	17.582	15.427	3.8118	3.0803	-1.609	4.1972	-14.7	-9.304	4.2995	-5.087
HPBW	79.653	95.12	83.423	58.508	75.255	72.807	93.496	82.4	67.99	57.735	83.551	41.747	79.217	28.094	74.267

(c)

No.	46	47	48	49	50	51	52	53	54	55	56	57	58	59	60
S11	-0.821	-6.544	-0.826	-5.466	-5.951	-1.926	-4.874	-5.869	-0.82	-5.457	-1.171	-1.159	-9.906	-2.763	-5.066
RA	3.2298	79.221	3.2534	21.512	26.194	8.7963	38.128	32.973	3.2217	19.264	146.44	131.66	78.884	34.965	64.547
XA	29.683	61.79	29.749	-29.49	34.685	-37.84	59.928	45.007	29.598	23.523	-296	-285.5	32.544	-88.17	76.064
HPBW	80.208	66.829	76.591	88.254	106.18	69.525	63.672	69.969	81.124	119.77	67.349	72.421	73.086	78.759	60.897

(d)

Table 4.2: The test dataset for the learning machine: (a) the S11 satisfies: $S11 < -15$ dB; (b) the resistance R_A satisfies: $40 < R_A < 60$ Ohm; (c) the reactance satisfies: $-20 < X_A < 20$ Ohm; (d) the HPBW satisfies: $HPBW > 60$ degree

4.2.2. Neural Network Model

The neural network in this project is built using MATLAB Neural Network Toolbox[16]. Considering the input space is only using nine dimensions, the neural network should not be too complicated. Otherwise, it may cause serious over fitting problem. The number of hidden layer should be limited under three and the number of neurons in each layer should also not be too large. But the exact setting of the network depends on the algorithm that is applied and it also needs to be verified after a series of experiments.

Training function

In [51], the available algorithms on MATLAB are described. The NN toolbox provides a total of 17 options on the training functions. However, there is no easier way to tell which algorithm is the best one for the given project. Hence, all the functions are applied roughly at the beginning. Their training results and relative costs are compared and five of them seem to be promising. Different from others, these five functions are able to provide convergent learning results and the fitting errors are comparable small. They are:

1. Bayesian Regularization ('trainbr'):

This one is currently the best performing algorithm. It can be applied to all the four learning objects and the mean squared error (mse) of the learning results are acceptable. The disadvantages are its relatively low training speed and inability to adjust the regularization parameter manually, which means it is hard to handle the generalization ability of the network.

2. Powell-Beale Conjugate Gradient Backpropagation ('traincgb'):

This training function seems to be promising, since the mse of training data can be very small, implying the fitting ability of the known data is quite good. However, the test error increases a lot, which

means the over fitting problem is worse. In general, this algorithm doesn't behave as good as Bayesian regularization on this problem.

3. Fletcher-Powell Conjugate Gradient Backpropagation ('traincgf'): Performance of 'traincgf' is comparable to last algorithm.
4. Levenberg-Marquardt Backpropagation ('trainlm'): This algorithm can also provide a satisfactory training result sometime. But the performances are not very constant in different training sessions, meaning the training results may be too haphazard. Another problem is it requires for too much computation memory and long computation time. Hence, less neurons but bigger regularization factor are applied. It may behave better on generalization.
5. Scaled Conjugate Gradient Backpropagation ('trainscg')

Through comparison, Bayesian regularization and Levenberg-Marquardt stand out. Actually, in [26], it also mentions that these two algorithms can obtain lower mse than any other algorithms for functioning approximation problem. At the end of that paper, the conclusion that Bayesian regularization method has a better performance than LM algorithm is drawn out. In their experiment, BR has the advantage on revealing potentially complex relationships. This conclusion is consistent with the experimental results of this thesis project. Thus, Bayesian regularization algorithm is applied for training the network.

Network structure and other parameters

As it is said in the beginning of this section, the neural network for this project should not be too complicated. So the network starts growing from one hidden layer and finally it is set as three hidden layers to obtain the best fitting ability. The numbers of neurons for the layers are 15, 25 and 20 respectively. The network structure can be simply expressed by figure 4.7. Transfer functions between hidden layers are set as sigmoid

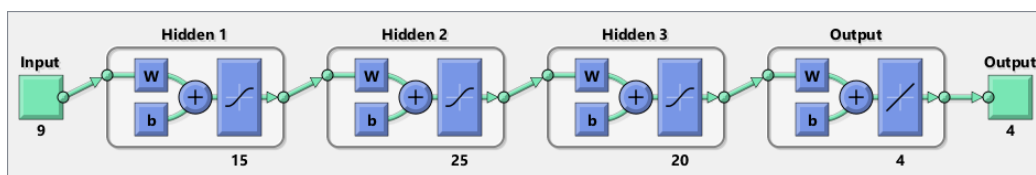


Figure 4.7: Structure diagram of neural network created by Matlab 2018a

function. Learning rate is 0.01. Mean squared error (mse) is used to estimate the network performance on MATLAB. During the training process, the training dataset is randomly divided into, "training", "validation" and "testing", three groups according to the ratios of 0.6, 0.2 and 0.2 respectively.

4.2.3. Support Vector Machine Model

The SVM model is constructed based on *LIBSVM*[8], a library for SVM, which is provided by Prof. C. Chang and Prof. C. Lin. The model itself is complete except for specific parameter setting of the library. Since SVM is not a usual machine learning model for regression problem as it is introduced in Chapter 3, the training process starts from the very simple scenario. That is to only input two features to the model at first. The height (H) and the length (L) of the dielectric cube are selected as input features, while others keep the same during the first training session.

The type of svm is chosen as *epsilon SVM*, which is normally used for regression problem. Besides, through multiple of tests, *Radial Basis Function (RBF)* is found out to be the most suitable kernel function. Other parameters are decided through cross validation method. For examples, the degree (d) of kernel is 7. Epsilon for loss function is 0.01 and the tolerance of termination criterion is 0.001.

4.2.4. Comparison between Two Models

Support vector machine model

In the former period of the project, SVM with two input features is firstly built. Since there are only two dimensions of the input space, the data distribution is easily displayed by plot. Take reflection factor (S11) of

antenna as an example (see figure 4.8):

It is obviously that the S11 of RDRA is changed according to some rules. Hence, it is supposed to be a simple

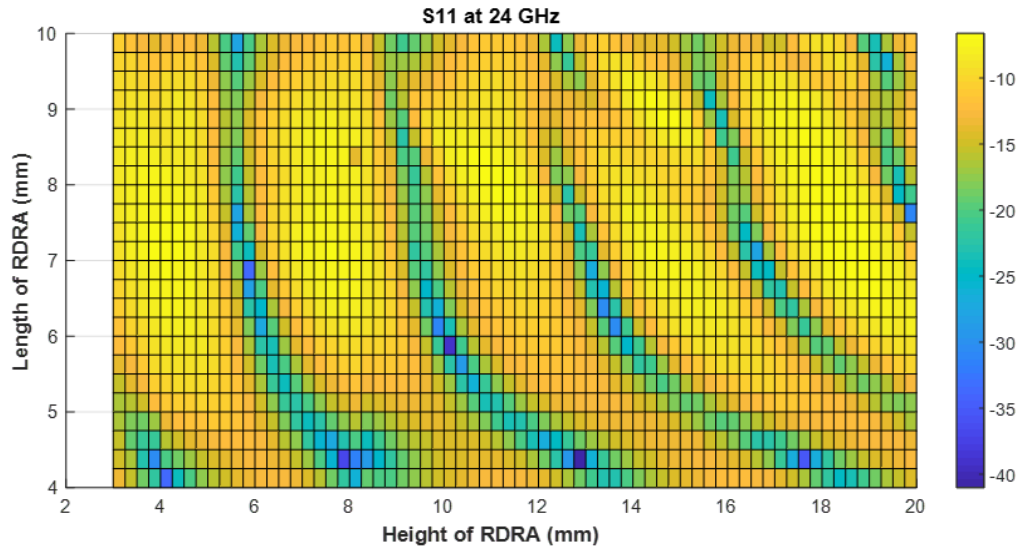


Figure 4.8: How S11 of RDRA distribute with changing H and L

pattern for SVM. Half of this dataset (862 sets) is used to train a SVM model and the rest of data (863 sets) can check the learning accuracy. Also, take result of learning S11 as a instance, the SVM performance is shown in figure 4.9.

The mean squared error of this model is 4.217 and the squared correlation coefficient is about 0.84. In figure 4.9, most of the predicted points are well matched to the points in the dataset. Some points that are very small, like those below -25 dB, may be regarded as out-liners, so the model quit fitting those points that much. In general, the model functions well for this simple input space. This is also a motivation for deeper study on SVM.

However, when the author tried to input all the features, the SVM model cannot give a satisfactory learning result no matter how the author adjusts the model parameters. Until this report was written, most of the trains did not provide a model that is convergent. Others were abandoned because of the too large mse and very low squared correlation coefficient.

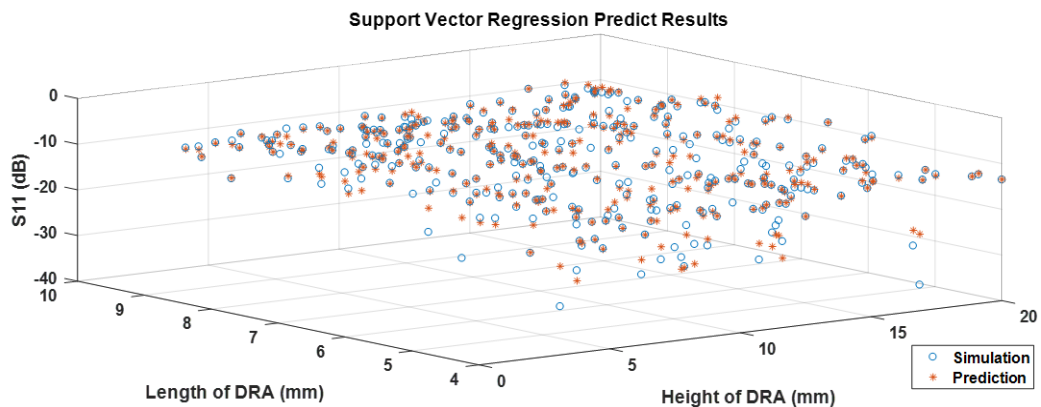
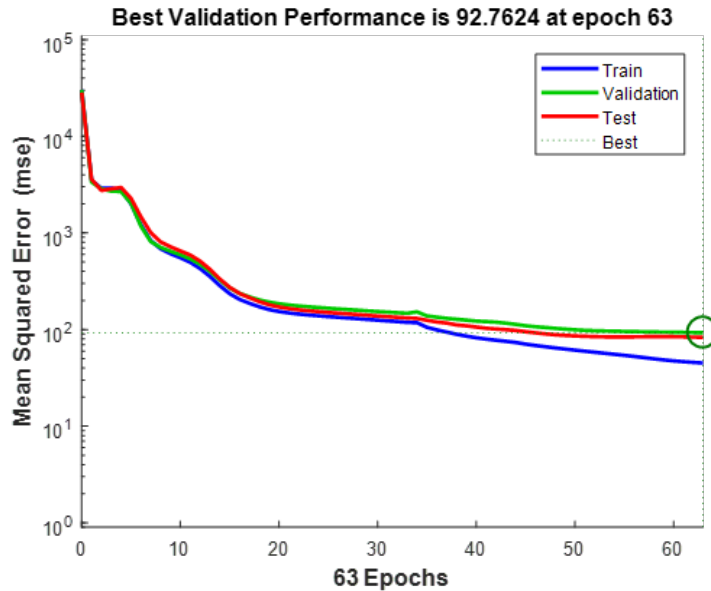


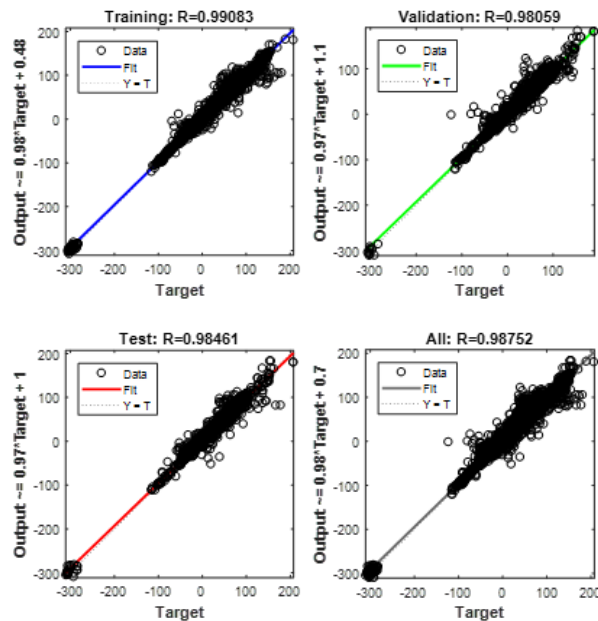
Figure 4.9: The prediction results on S11 of support vector regression model

Neural network model

After trying to apply SVM method, the attention is transferred to neural network. The basic network parameters and structures are demonstrated in the former section. Here, some training results will be provided. Different from the SVM, neural network is better at dealing with high dimensional regression problems. So the network directly begin with being trained by all the input features in this project and output the four antenna performance indexes (S11, Rin, Xin, HPBW) together. The network performance is commented by the mse of validation data group and the regression levels in figure 4.10. It can be seen that after around 50th



(a) Performance during training



(b) Regression of training results

Figure 4.10: The performance of neural network 1.0 version

training epoch, the validation performance cannot be improved within another 15 epochs and the best performance for all these four outcome is mse equaling 92.76. On the other hand, the regression levels are quite satisfying, since for all the groups of data, the regression coefficient can attain as high as 0.98, implying that

	S11	Rin	Xin	HPBW
mean error	3.16 dB	6.99 Ω	7.58 Ω	6.66°

Table 4.3: Mean error of test data for neural network version 1.0

the network learning results are highly close to the data which are computed by CST.

After the training process is done, the network is test by the independent data group (recorded in table 4.2). The test outcomes are shown in figure 4.11. Clearly the neural network behaves much better on fitting the antenna performance. The blue lines, connecting the outcome points of the test data, are well correspond to the red lines. The mean error for each index is shown in table 4.3.

According to the requirements for the models, the results of the first version of network are acceptable. The learning results of antenna reactance and 3dB angular beamwidth can achieve the standard. Yet, for reflect factor and antenna resistance, the errors are slightly beyond the upper-limitation. What's more, the first sub-plot in figure 4.11 shows that the network is weak at predicting in the area where s11 is smaller than -15 dB. The same thing happens to the prediction of the antenna resistance. Learning ability of the network seems to be weakened around 50 Ohm. These problems absolutely increase the test error and related solutions will be discussed in the later section.

4.2.5. A short summary

Without doubt, neural network is a better machine learning method for this project. It shows the superiority both in network training speed and training accuracy. Thus, in the later sections of the report, only neural network will be left for studying and discussing.

4.3. Optimization of Training Model

Although the first version of neural network can provide some good predictions, it still can't fulfill all the requirements. In order to improve it, two solutions are put forward.

4.3.1. Separation of learning objects

The neural network version 1.0 integrated four learning objects in the outcome matrix. That means the network has to recognize the relationships between input features and the four objects. During the training process, the network may have the trend to fit the majority of the data. This may result the tolerance for the data group which doesn't occupy a big ratio among the dataset. For example, the variant range of S11 is about -40 dB to 0 dB, while the range for reactance may attain to -300 Ohm to 300 Ohm. In order to decrease the validation error, the network may add heavier weight on learning the reactance. oppositely it will reduce the punish on the errors of S11. Hence, the idea to separate the learning objects in different networks is came up with. According to these four different objects, four networks are constructed and their parameters are also adjusted. Then test by the same dataset as it is used before, the learning results are updated in figure 4.12.

Obviously, the network for S11 is improved a lot. Though the predict error is still likely bigger in the area where $S_{11} < -15$ dB, the difference between prediction results and simulation data is much less compared to the result in figure 4.11. The mean error for each index is also computed in table 4.4

	S11	Rin	Xin	HPBW
mean error	2.17 dB	3.23 Ω	7.76 Ω	4.90°

Table 4.4: Mean error of test data for neural network version 2.0

4.3.2. Imbalance data distribution problem

After retraining the four networks separately, the prediction errors are all smaller than the setting value. Especially, the improvement on estimating S11 is remarkable. However, the fitting ability is still worse when

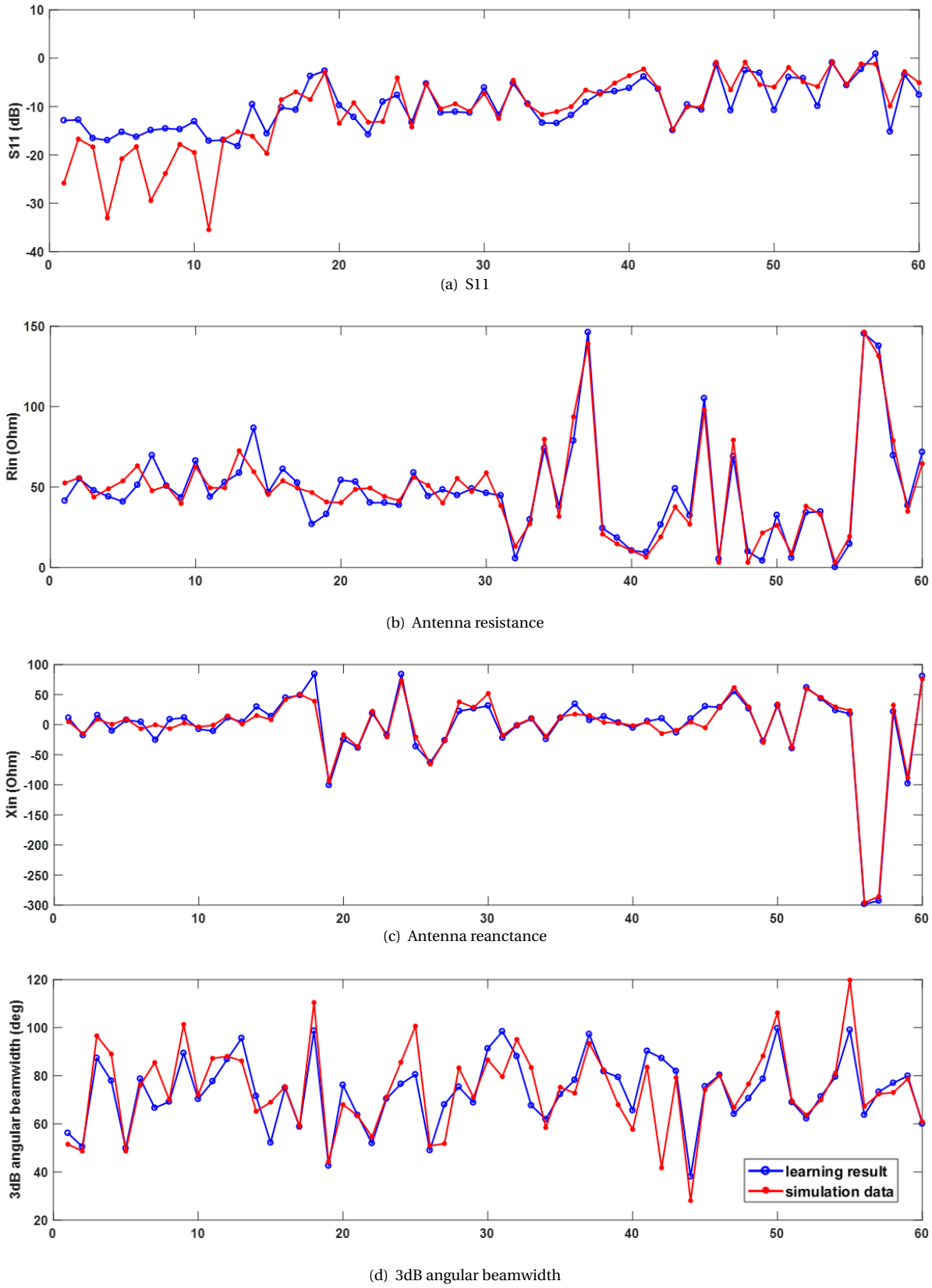


Figure 4.11: The test results of neural network 1.0 version

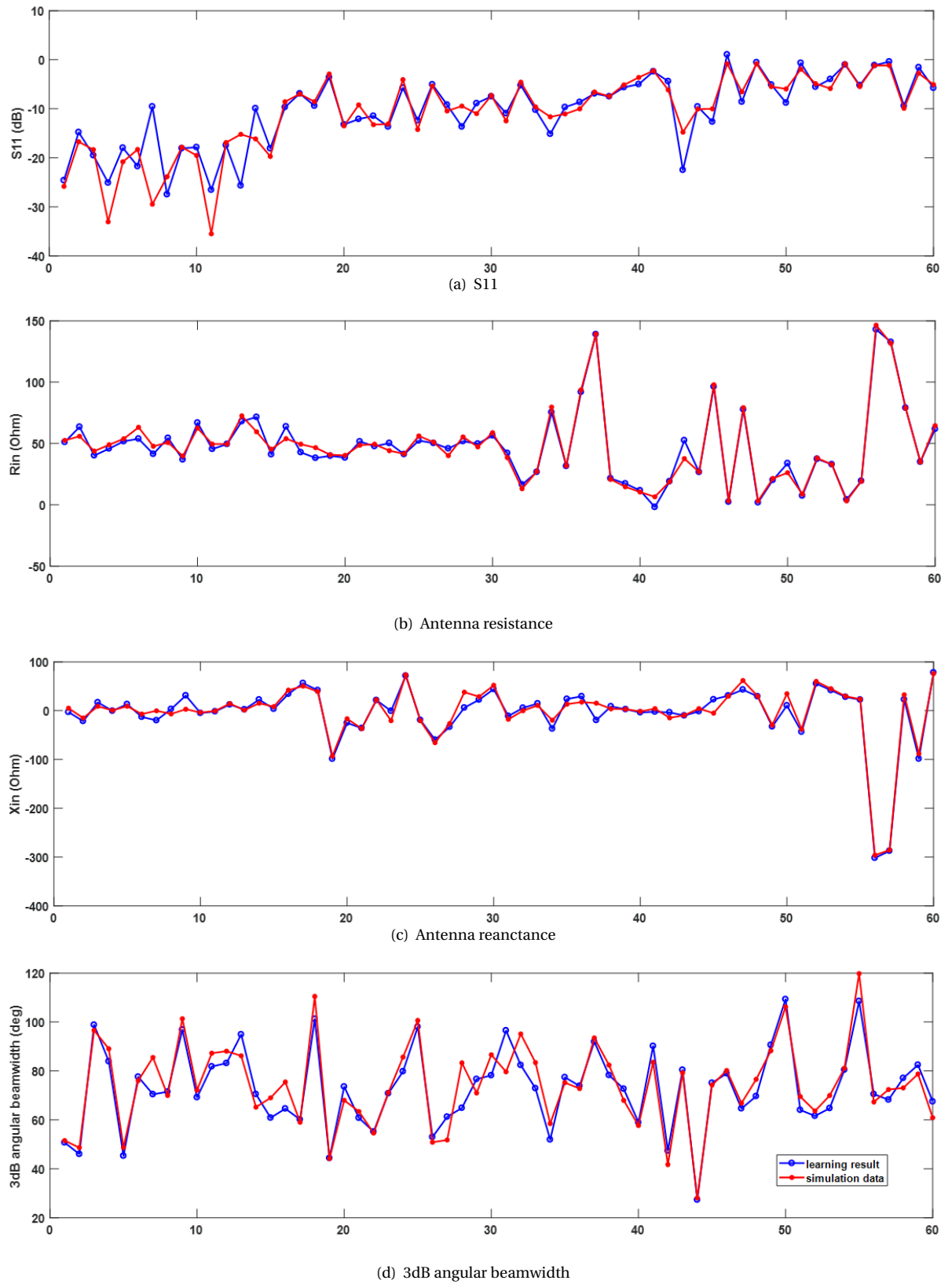


Figure 4.12: The test results of neural network 2.0 version

S11 is smaller than -15 dB, where the mean error of the test data is around 4.78 dB. The hypothesis is that the amount of training data is relatively insufficient in that area. Thus, the distribution of training data is verified by plotting, shown in figure 4.13.

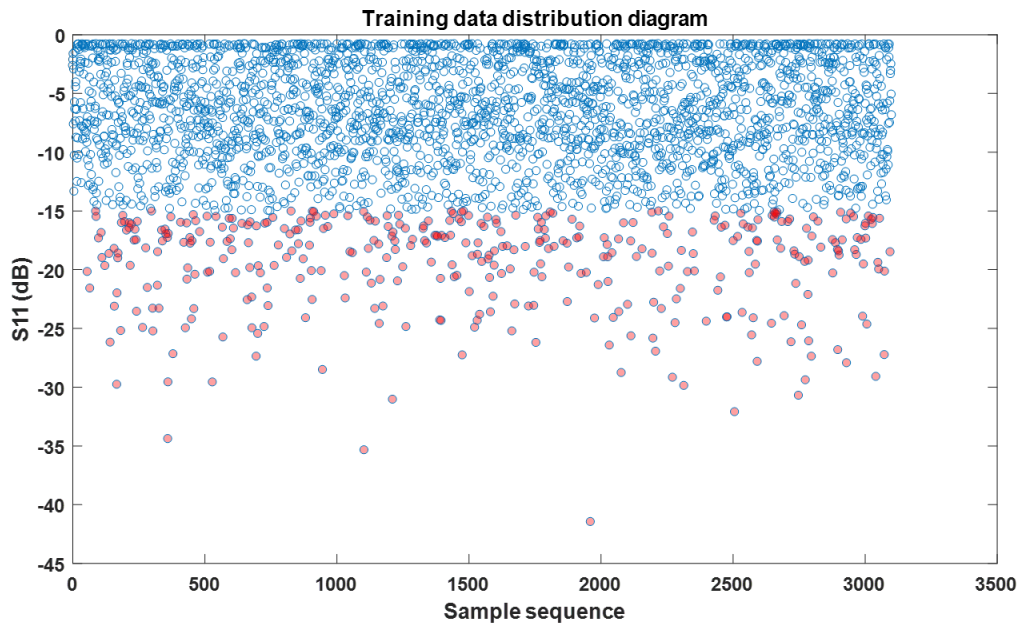


Figure 4.13: The distribution diagram of training data

Obviously, only a small percentage of the training data, can provide S11 that is below -15 dB (expressed by red points). The total number of these data is only 385, only around one tenth of the whole dataset. So the imbalance distribution problem of training data is supposed to exist. In paper [20], several methods are introduced to figure out this problem. In this project, the *Under-sampling* method is taken. The action needs to be done is to extract some samples randomly from most classes so as to reduce the number of samples in these classes and make the sample data reach a relative balance. Under-sampling can be thought as the easiest way to solve the imbalance data problem.

Hence, the training dataset is divided into two groups, named "good" and "bad". For the good group, there are 976 sets of data that can output the S11 below -10 dB, while the bad group contains all other data. A new training dataset is made up by combining the good group and the data randomly chosen from the bad group. Finally, the network trained by the good group and another 1551 sets of data from the bad group is shown

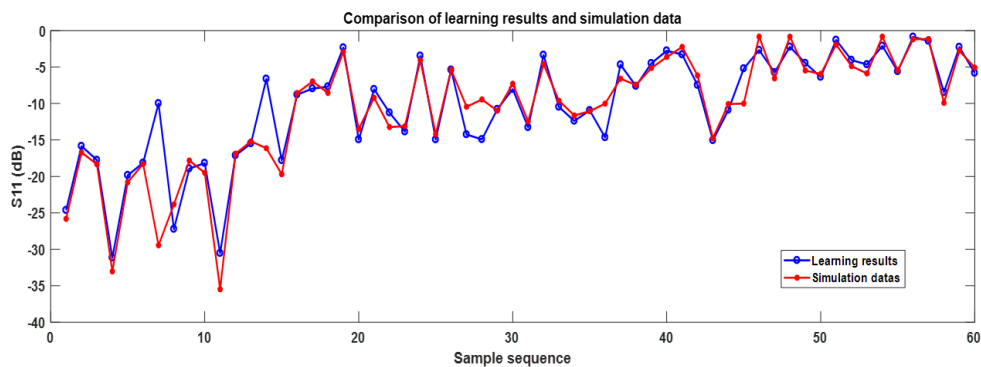


Figure 4.14: Mean error of test data (S11) for neural network version 3.0

in figure 4.14. The mean error of these 60 sets of data is 1.68 dB, reducing 22.6% from prediction error of network version 2.0. What is more important is that for the first 15 sets of data, where the S11 is below -15

dB, the average error is 3.19 dB now. So the network prediction errors are decreased after adjusting the data distribution.

What should be stated is that the imbalanced data distribution problem is sharp only for S11. That's why only the training dataset used for predicting S11 is under sampling and reshaped beforehand in this project, while others remain the same. Now the prediction errors are show in table 4.5

	S11	Rin	Xin	HPBW
mean error	1.68 dB	3.23 Ω	7.76 Ω	4.90°

Table 4.5: Mean error of test data for neural network version 3.0

4.4. Conclusion

In this chapter, the whole process about constructing a proper learning model has been illustrated. At the beginning, it specified some basic definitions of rectangular dielectric resonant antenna, clarifying the indicators for estimating the performance of an antenna. Three of them are selected to be the prediction objects of the learning model. They are the antenna reflection coefficient, input impedance and 3 dB angular beamwidth. In the same section, nine design parameters of the antenna, which are also the input features for the model, are introduced. In table 4.1, the design space of each feature is concluded. According to the input features and output prediction objects, 3161 sets of data are collected by simulating the antenna topologies on the software CST. Among these data, 60 sets are separated to be used as test data and the rest of the data can be used for training model.

The second section, the standards for the final model are put forwarded firstly. They state that the final model should be checked by the test data group and confine the boundaries of prediction errors. After the requirements are clarified, the process of constructing the neural network and SVM models are displayed, followed by their performance. Through comparison between these two machine learning methods, neural network is chosen for the further study and application. The neural network is capable of dealing with the complicated relationships between the nine input features and providing a promising prediction result.

Learning objective	Network hidden layer			test error
	layer 1	layer 2	layer 3	
S11	20	20	20	1.68 dB
Rin	25	20	25	3.23 Ω
Xin	20	25	25	7.76 Ω
HPBW	15	25	20	4.9°

Table 4.6: Structure and performance of the final neural network

The third section focused on analyzing and optimizing the built neural network. The first action is to build independent network for each learning object instead of output all the four indexes by one NN. This is because the network will attempt to decrease the overall error while the local correctness is neglected sometimes. The same mistake may also be caused by imbalance data distribution. Hence, another step is to adjust the data ratio to make the training data more even. After these two improvements, the network can satisfy the requirements of the model. That means the model prediction error can achieve following standards:

1. For reflector factor: $Mean\ error_{S11} < 3\ dB$
2. For resistance of antenna: $Mean\ error_{Rin} < 5\ \Omega$
3. For reactance of antenna: $Mean\ error_{Xin} < 10\ \Omega$
4. For 3dB angular beamwidth of antenna: $Mean\ error_{HPBW} < 10^\circ$

In conclusion, the learning model, based on neural network, for estimating the performances of RDRA under different design conditions is now constructed. The preset requirements for this model can all be satisfied. The networks' structure and prediction performances are concluded in table 4.6. The neural networks for all of the four learning objectives are trained by Bayesian Regularization algorithm. The activation functions between layers are using sigmoid function.

In the next chapter, practical experiments will be designed and implemented to verify the simulation reliability and learning model accuracy.

5

Experiment Verification

In the former chapter, the neural network is verified by 60 sets of data. In this project, 10 antenna prototypes are designed to verify the simulation accuracy.

5.1. RDRA Prototype Design

The prototypes are designed under the confinements which are introduced in Chapter 4. Since the dimensions of the resonator cube and the size of ground plane are the mostly vulnerable to change and they are also easily modulated in practical, these ten prototypes are different in their resonator and ground plane size. In other word, the feedline structure and the resonator material keep consistent.

L_{stub} is 2.3 mm. This length is slightly shorter than a quarter of wavelength (24 GHz). In theory, the power can be well fed to the aperture. The resonator material is polycarbonate[54]. This cheap material are widely used in human life, such as the lamp covers. Also, due to its good electrical insulator, heat resistant and flame-retardant properties, this material fits the application in the project quite well. The only thing is that there was no reliable data of the relative dielectric constant of this material at 24 GHz. However, my colleagues, John and Mai-Han measured the missing data in the Signify lab. Their conclusion is that the ϵ_r of this material is around 2.5 to 2.6 at 24 GHz. Thus, in this project, the input feature, ϵ_r is set as 2.55.

5.1.1. Design of Rectangular DRA

There are six dielectric cubes with different sizes. The dimension values are arbitrarily chosen in the interval from 3 mm to 10 mm. They are shown in figure 5.1(a). Besides, in table 5.1, the exact dimensions of cubes can be found.

No	Height(H)	Length(L)	Width(W)
1	8	5	4.9
2	9	8.1	8.1
3	10	8.1	6.1
4	4.1	8.1	8.1
5	8.1	4	10
6	6.1	5.1	5.1

Table 5.1: The dimensions of resonator cubes in measurements

As can be seen in figure 5.1(b), the PCBs (Printed Circuit Boards) of the prototypes are cut in three directions. They are dx_p , dx_n and dy_n (refer in figure 4.5). In this way, ground planes with different sizes can be attained. The reason for dy_p stays the same is because the feed circuit will only be connected to this side, for the purpose to save the expense of making prototypes. In table 5.2, five different sets are demonstrated.

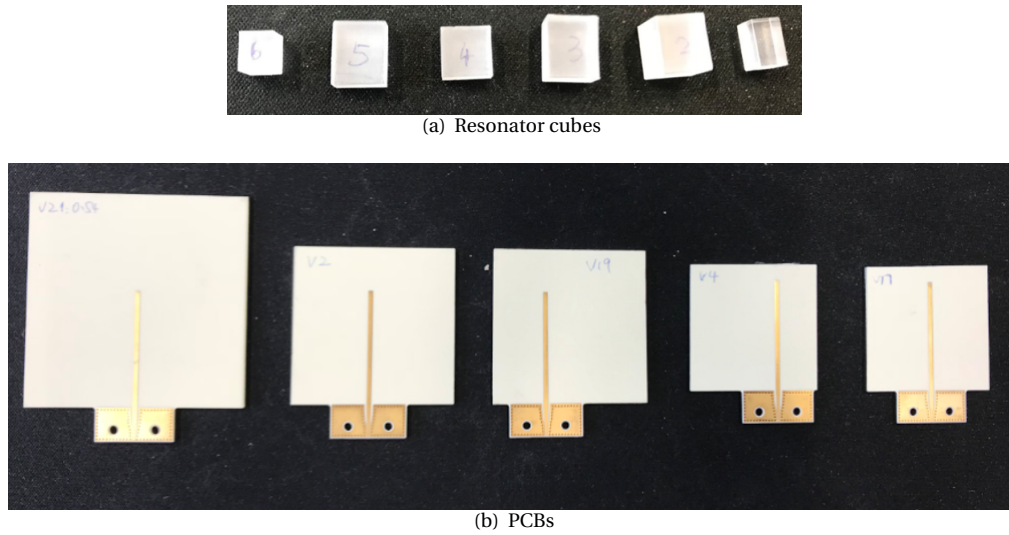


Figure 5.1: Dielectric cubes and PCBs of DRA prototypes

No	dx_n	dx_p	dy_n	dy_p
1	21.25	10	6.25	25
2	15	16.25	6.25	25
3	18	19.5	12.5	25
4	12.5	25	12.5	25
5	25	25	25	25

Table 5.2: The dimensions of ground plane in measurements

Randomly combine the six cubes and five PCBs, thirty groups of prototypes can be formed. Due to the limited time, ten of them were measured in DUCAT, with the help of Mr. Pascal Aubry.

5.1.2. Design of Grounded Co-planar Waveguide

In order to feed the antenna prototypes, the microstrip feedline will be connected by coaxial line. The end launch connector, 1092-01A-5, from Southwest Microwave is adopted (shown in figure 5.2).

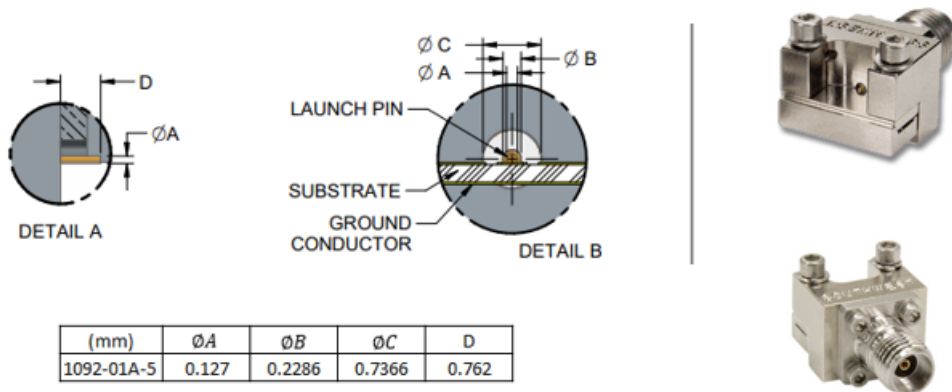


Figure 5.2: Launch end connector 1092-01A-5 from Southwest Microwave

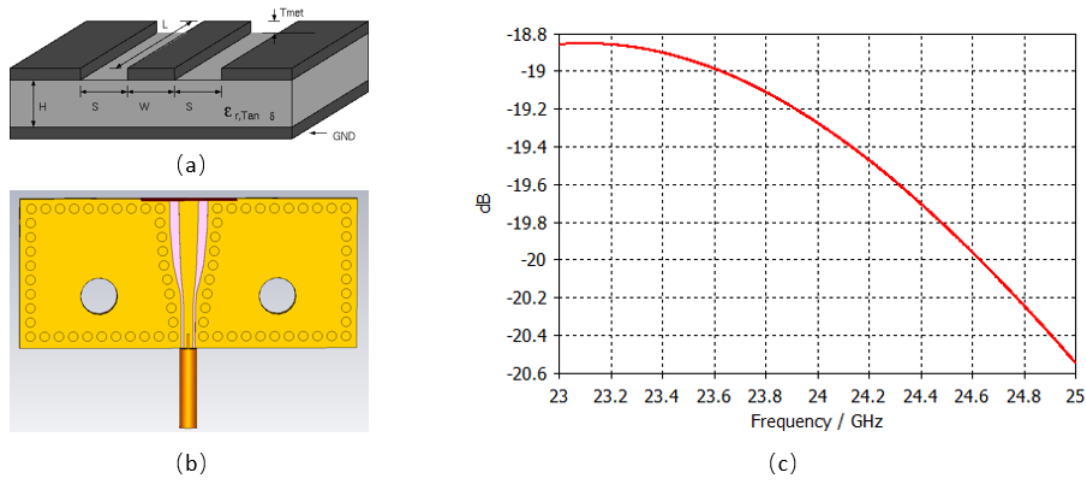


Figure 5.3: Converter between coaxial input and antenna PCB: (a) GCPW sketch ([9]); (b) CST model of the the converter circuit; (c) S parameter (S11: magnitude in dB) of the converter circuit

As the connector pin diameter A is only 0.127 mm, which mismatches the feedline width (1.05 mm), the remarkable reflection may be caused at the connected spot. For the purposes of decreasing the error brought in by circuit mismatching, a grounded coplanar waveguide (GCPW) circuit is inserted between antenna PCB and the coaxial connector. By this method, the center feedline width is narrowed gradually.

In [9], the field analysis of GCPW and how to calculate its topology structure are specified. Given the H , T_{met} , and ϵ_r , then the microstrip width W can be adjusted by changing the trace width S (ref figure 5.3 (a)). Decreasing the S and W with small step size, the converter can finally be obtained. In the figure 5.3 (c), it implies that the converter circuit can match to 50 Ohm very well at 24 GHz, since the s_{11} is the way below than -10 dB. In this way, it is assumed that the converter will not interfere the antenna that much. Now all the parts of the RDRA prototypes have been declared. The resonator plastic cube, microstrip line PCB and the converter circuit will be assembled. 10 combinations will be finally measured in DUCAT. A example prototype is shown in figure 5.4.



Figure 5.4: RDRA prototype for measurement

5.2. Measurement Results and Analysis

What should be clarified is that only S11 and the radiation pattern can be directly measured in the laboratory. As for antenna input impedance, it can be computed through equation 4.4.

NO	H(mm)	L(mm)	W(mm)	dx_n(mm)	dx_p(mm)	dy_n(mm)	dy_p(mm)	S11(dB)	HPBW(deg)	
1	8	5	4.9	25	25	25	25	-19.26	68	S
								-13.26	60	M
								-19.31	57.36	P
2	9	8.1	8.1	12.5	25	12.5	25	-9.32	59.4	S
								-19.39	53	M
								-10.17	60.48	P
3	6.1	5.1	5.1	18	19.5	12.5	25	-14.94	111.4	S
								-16.43	76	M
								-17.63	106.07	P
4	10	8.1	6.1	15	16.25	6.25	25	-12.3	59	S
								-19.33	57	M
								-10.19	54.86	P
5	4.1	8.1	8.1	21.25	10	6.25	25	-9.44	93.6	S
								-14.42	86	M
								-9.47	80.4	P
6	6.1	5.1	5.1	25	25	25	25	-14.79	109	S
								-15.46	96	M
								-10.79	100.44	P
7	8.1	10	6.1	12.5	25	12.5	25	-13.83	51.7	S
								-13.16	48	M
								-17.71	52.07	P
8	8.1	4	10	18	19.5	12.5	25	-12.07	59.9	S
								-14.14	74	M
								-16.63	63.79	P
9	5	8	4.9	15	16.25	6.25	25	-15.14	85.1	S
								-14.74	63	M
								-12.27	78.37	P
10	9.1	8.1	8.1	21.25	10	6.25	25	-9.56	59.3	S
								-15.89	57	M
								-11.11	56.15	P

Table 5.3: Measurement results of RDRA prototypes ($\epsilon_r = 2.55$, $L_{stub} = 2.3mm$)

Table 5.3 records the 10 samples. The simulation, measurement and neural network prediction results are all included. "S", "M" and "P" in the table represent simulation, measurement and prediction respectively. Figure 5.5 shows the radiation patterns of these prototypes. Besides, in order to have a more intuitive assessment, the histograms of these prototypes are given in figure 5.6 (a) and figure 5.6 (b).

For these ten prototypes, the mean prediction errors is **2.26 dB** for S11 and **5.07 degree** for HPBW. Clearly, the prediction results of neural network can fulfill the requirements for this model and provide a good estimation of antenna performance.

However, there are obvious differences between simulation and practical measurement. In figure 5.5, some radiation patterns are shifted. Also, simulation values of S11 and HPBW sometimes have relatively big error to measurements. For example, the second, fourth, fifth and tenth samples in figure 5.6 (a).

Reasons do exist for these differences. As it is mentioned in last section, a CPW circuit is inserted between the antenna PCBs and the coaxial connector. Hence, insert loss cannot be avoid. Another reason is that the measurement error caused by prototype manufacturing and equipment measuring accuracy. The last but not the least, the relative dielectric constant ϵ_r of the resonator is roughly measured at 24 GHz due to the limited measurement condition. The exact value of ϵ_r may be different from what is used in the simulations.

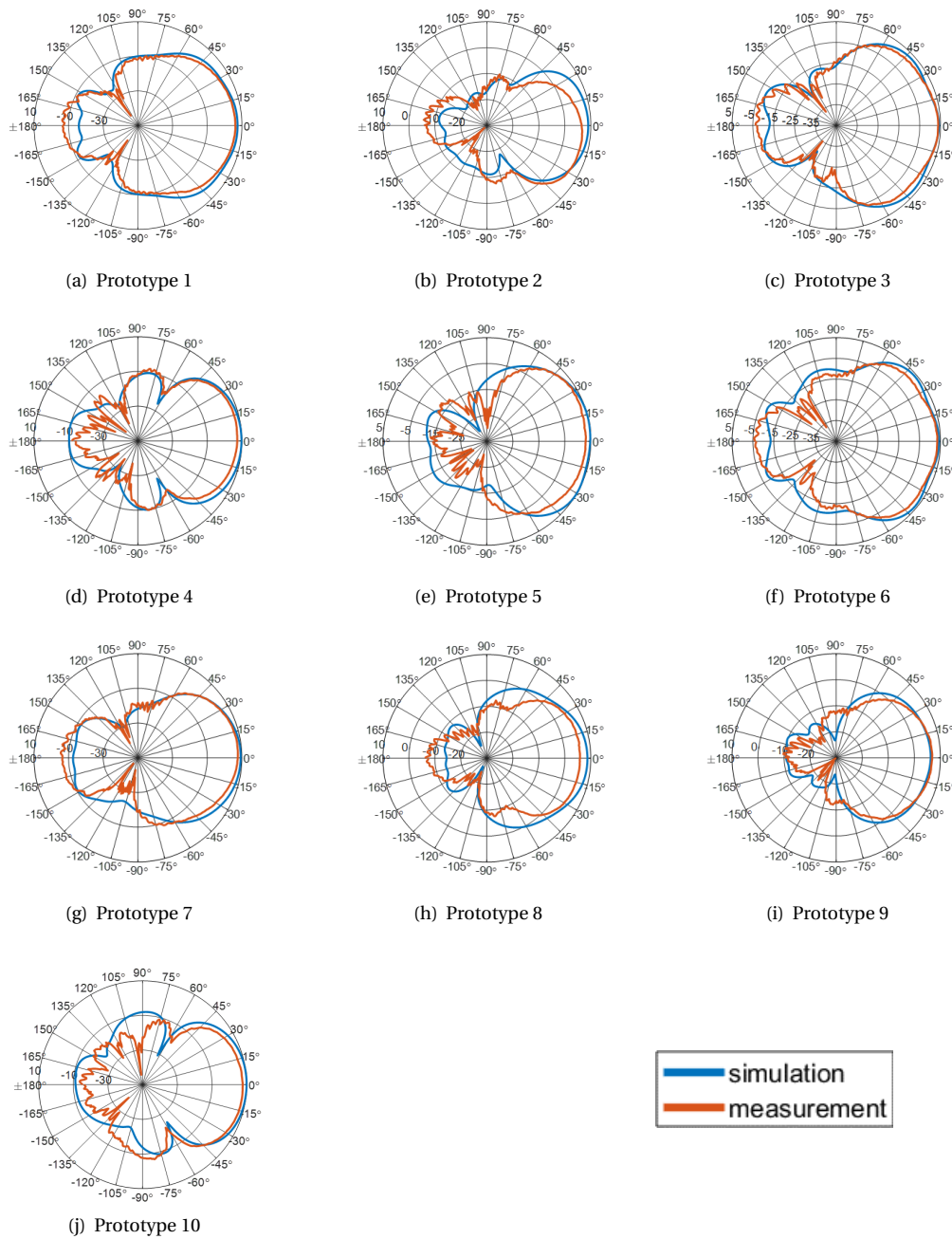


Figure 5.5: Radiation patterns in H cut of ten RDRA prototypes

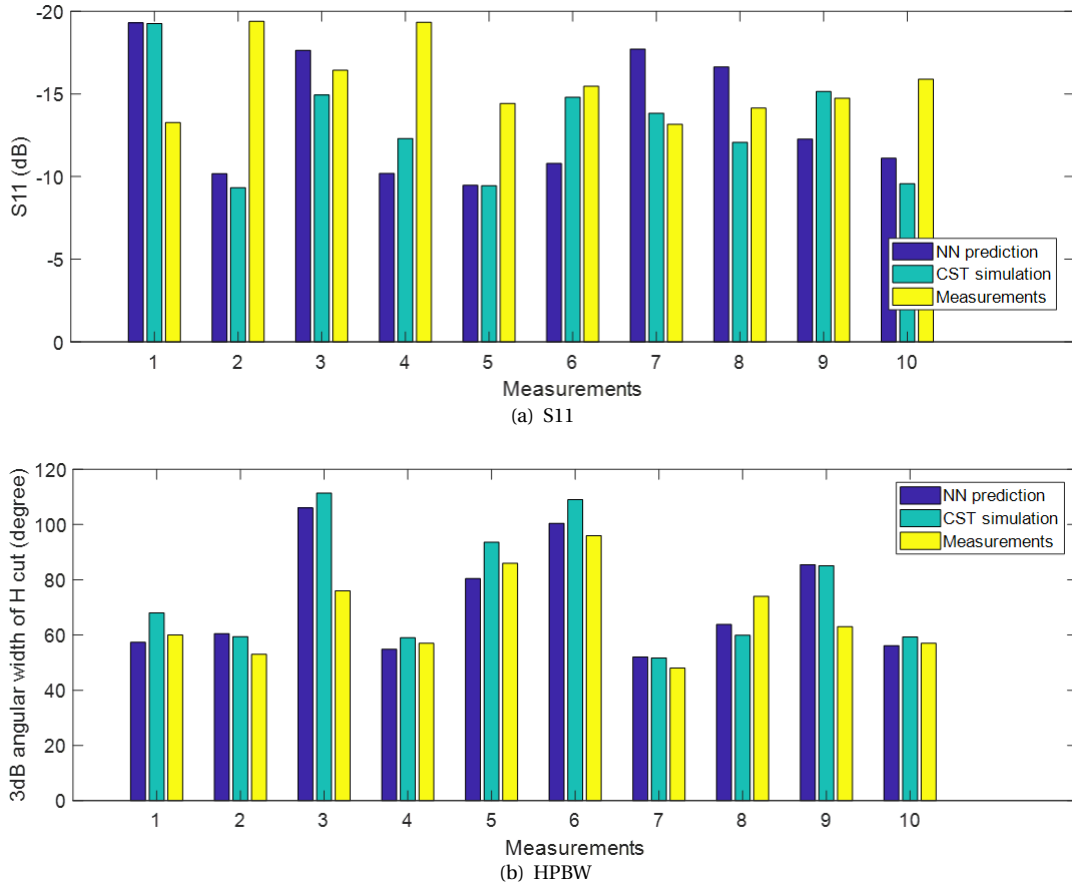


Figure 5.6: Comparison of NN prediction, CST simulation and measurements for RDRA prototypes: (a) Comparison result of S11; (b) Comparison result of HPBW

5.3. Conclusion

The chapter specifies the physical verification process for the antenna simulation models and the prediction accuracy of the neural networks which are developed in Chapter 4.

In total, ten antenna prototypes were designed. Their reflection coefficients and radiation patterns in H cut were measured in DUCAT of MS3 group at TU Delft. They have dielectric resonators with different dimensions and orientations, also their ground plane sizes are not the same. The detailed prototype parameters can be found in table 5.3. In the same table, the results of simulation, neural network predictions and experimental measurements for these ten prototypes were also recorded. The differences among NN prediction, CST simulation and measurements are intuitively reflected in figure 5.6.

For S11, the averaged prediction error of the neural network model is 2.26 dB. For HPBW, the mean error of NN is 5.07 degree. Both of them have achieved the goals of the learning model. Besides, most of the measurements are in good agreement with the simulation results. The existed differences can be accepted when consider the influence of the inserted CPW, the uncertain dielectric constance of the resonator and measurement errors. In a word, the practical measurements of the antenna prototypes further verified the feasibility of this thesis.

6

Conclusion and Future Work

6.1. Conclusion

In this master project, a neural network-based model for estimating the performance of rectangular dielectric resonant antenna has been developed. To be specific, the neural networks that constructed in this project can predict the reflection factor, input impedance and 3dB angular beamwidth of the RDRA while the antenna's topology is changed according to its ground plane, feed structure and resonator cube.

The network model was trained by 3101 sets of simulation data in total and the model performances were checked by another 60 sets of data. The final test errors for four objects all achieved the goals. Experiments of ten RDRA prototypes were designed and implemented. The reliability of the simulation data and the prediction accuracy of the neural network model have been successfully verified by the experiments.

This thesis realized a bold and novel attempt: apply machine learning theory to model and assess the rectangular dielectric resonant antenna under such a high dimensional design space. With limited amount of simulation data, the neural network was trained to predict the antenna performance accurately. With further work, it is promising to apply this neural network model as a good assessment tool for designing RDRA.

6.2. Future Work

In this thesis, the potential of applying machine learning technology on antenna performance estimation is shown. Though there are still many limitations to combining these two fields. The remain problems and future study are suggested as below:

1. The training dataset should be distributed more evenly and sparse. In this way, a wider design space can be applicable.
2. Antenna should be assessed from more aspects, like the bandwidth and gain. Hence, the neural network can be trained to learning more objectives.

Bibliography

- [1] Anonymous. Distance formula and pythagorean theorem. http://www.mathwarehouse.com/algebra/distance_formula. Accessed 2nd. August, 2018.
- [2] A Axelrod, M Kisliuk, and J Maoz. Broadband microstrip-fed slot radiator. *Microwave Journal*, 32:81, 1989.
- [3] Robert Berwick. An idiot's guide to support vector machines (svms).
- [4] SA Billings and QM Zhu. Model validation tests for multivariable nonlinear models including neural networks. *International Journal of Control*, 62(4):749–766, 1995.
- [5] Christopher JC Burges. A tutorial on support vector machines for pattern recognition. *Data mining and knowledge discovery*, 2(2):121–167, 1998.
- [6] Gail A. Carpenter and Stephen Grossberg. The art of adaptive pattern recognition by a self-organizing neural network. *Computer*, 21(3):77–88, 1988.
- [7] Keith Carver and James Mink. Microstrip antenna technology. *IEEE transactions on antennas and propagation*, 29(1):2–24, 1981.
- [8] Chih-Chung Chang and Chih-Jen Lin. Libsvm: a library for support vector machines. *ACM transactions on intelligent systems and technology (TIST)*, 2(3):27, 2011.
- [9] Kai Chang. *RF and microwave wireless systems*, volume 161. John Wiley & Sons, 2004.
- [10] Assistant Prof. Chen. The basis concept of svm. <https://zhuanlan.zhihu.com/p/24638007>. Accessed 2nd. August, 2018.
- [11] Xiao Hui Chen, Xin Xin Guo, Jin Ming Pei, and Wen Yi Man. A hybrid algorithm of differential evolution and machine learning for electromagnetic structure optimization. In *Automation (YAC), 2017 32nd Youth Academic Annual Conference of Chinese Association of*, pages 755–759. IEEE, 2017.
- [12] A Balanis Constantine et al. Antenna theory: analysis and design. *MICROSTRIP ANTENNAS, third edition*, John wiley & sons, 2005.
- [13] Rogers Corporation. Rogers ro 4350b data sheet. <https://www.rogerscorp.com/documents/887/acs/R04003C-and-R04350B-Laminates-with-TICER-Foil.pdf>. Accessed 26th. August, 2018.
- [14] George Cybenko. Approximation by superpositions of a sigmoidal function. *Mathematics of control, signals and systems*, 2(4):303–314, 1989.
- [15] Richard D De Veaux and Lyle H Ungar. A brief introduction to neural networks. *Unpublished: http://www.cis.upenn.edu/~ungar/papers/nnet-intro.ps*, 1997.
- [16] Howard Demuth and Mark Beale. Neural network toolbox for use with matlab – user's guide verion 3.0, 1993.
- [17] Rong-En Fan, Pai-Hsuen Chen, and Chih-Jen Lin. Working set selection using second order information for training support vector machines. *Journal of machine learning research*, 6(Dec):1889–1918, 2005.
- [18] Bratin Ghosh, Kunal Ghosh, and Chandra Sekhar Panda. Coplanar waveguide feed to the hemispherical dra. *IEEE Transactions on Antennas and Propagation*, 57(5):1567–1571, 2009.
- [19] Simon S Haykin, Simon S Haykin, Simon S Haykin, and Simon S Haykin. *Neural networks and learning machines*, volume 3. Pearson Upper Saddle River, NJ, USA:, 2009.

- [20] Haibo He and Edwardo A Garcia. Learning from imbalanced data. *IEEE Transactions on knowledge and data engineering*, 21(9):1263–1284, 2009.
- [21] Donald O Hebb et al. The organization of behavior, 1949.
- [22] Kurt Hornik, Maxwell Stinchcombe, and Halbert White. Multilayer feedforward networks are universal approximators. *Neural networks*, 2(5):359–366, 1989.
- [23] Maciej Huk. Backpropagation generalized delta rule for the selective attention sigma-if artificial neural network. *International Journal of Applied Mathematics and Computer Science*, 22(2):449–459, 2012.
- [24] Gregory P Junker, AA Kishk, and Allen W Glisson. Input impedance of dielectric resonator antennas excited by a coaxial probe. *IEEE Transactions on Antennas and Propagation*, 42(7):960–966, 1994.
- [25] D Kajfez and P Guillon. Dielectric resonators, norwood, ma: Artec house, 1986.
- [26] Murat Kayri. Predictive abilities of bayesian regularization and levenberg–marquardt algorithms in artificial neural networks: a comparative empirical study on social data. *Mathematical and Computational Applications*, 21(2):20, 2016.
- [27] S Keyrouz and D Caratelli. Dielectric resonator antennas: Basic concepts, design guidelines, and recent developments at millimeter-wave frequencies. *International Journal of Antennas and Propagation*, 2016, 2016.
- [28] Ahmed A Kishk and Wei Huang. Use of electric and magnetic conductors to reduce the dra size. In *Antenna Technology: Small and Smart Antennas Metamaterials and Applications, 2007. IWAT'07. International Workshop on*, pages 143–146. IEEE, 2007.
- [29] Alan H Kramer and Alberto Sangiovanni-Vincentelli. Efficient parallel learning algorithms for neural networks. In *Advances in neural information processing systems*, pages 40–48, 1989.
- [30] RA Kranenburg and SA Long. Microstrip transmission line excitation of dielectric resonator antennas. *Electronics Letters*, 24(18):1156–1157, 1988.
- [31] Roger A Kranenburg, Stuart A Long, and Jeffery T Williams. Coplanar waveguide excitation of dielectric resonator antennas. *IEEE Transactions on Antennas and Propagation*, 39(1):119–122, 1991.
- [32] Dave Krebs. Introduction to kernel methods. <https://people.cs.pitt.edu/~milos/courses/cs3750-Fall2007/lectures/class-kernels.pdf>. Accessed 8th. August, 2018.
- [33] KW Leung, KM Luk, and KYA Lai. Input impedance of hemispherical dielectric resonator antenna. *Electronics Letters*, 27(24):2259–2260, 1991.
- [34] KW Leung, KM Luk, KYA Lai, and D Lin. Theory and experiment of a coaxial probe fed hemispherical dielectric resonator antenna. *IEEE Transactions on Antennas and Propagation*, 41(10):1390–1398, 1993.
- [35] Kwok-Wa Leung, Kwai-Man Luk, Kin YA Lai, and Deyun Lin. Theory and experiment of an aperture-coupled hemispherical dielectric resonator antenna. *IEEE Transactions on Antennas and Propagation*, 43(11):1192–1198, 1995.
- [36] Kwok Wa Leung, Eng Hock Lim, and Xiao Sheng Fang. Dielectric resonator antennas: From the basic to the aesthetic. *Proceedings of the IEEE*, 100(7):2181–2193, 2012.
- [37] Eng Hock Lim and Kwok Wa Leung. Transparent dielectric resonator antennas for optical applications. *IEEE transactions on antennas and propagation*, 58(4):1054–1059, 2010.
- [38] Jianping Liu. Principles of support vector machine theory. <http://www.cnblogs.com/pinard/p/6113120.html>. Accessed 9th. August, 2018.
- [39] S Long, Mark McAllister, and Liang Shen. The resonant cylindrical dielectric cavity antenna. *IEEE Transactions on Antennas and Propagation*, 31(3):406–412, 1983.
- [40] Kwai Man Luk, Kwok Wa Leung, KM Luk, and KW Leung. Dielectric resonator antennas. 2002.

- [41] Enrique AJ Marcatili. Dielectric rectangular waveguide and directional coupler for integrated optics. *Bell Labs Technical Journal*, 48(7):2071–2102, 1969.
- [42] MW McAllister and S Andrew Long. Resonant hemispherical dielectric antenna. *Electronics Letters*, 20(16):657–659, 1984.
- [43] MW McAllister, S Andrew Long, and GL Conway. Rectangular dielectric resonator antenna. *Electronics Letters*, 19(6):218–219, 1983.
- [44] R Kumar Mongia and Apisak Ittipiboon. Theoretical and experimental investigations on rectangular dielectric resonator antennas. *IEEE Transactions on Antennas and Propagation*, 45(9):1348–1356, 1997.
- [45] RK Mongia, A Ittipiboon, and M Cuhaci. Low profile dielectric resonator antennas using a very high permittivity material. *Electronics letters*, 30(17):1362–1363, 1994.
- [46] Frank Rosenblatt. Principles of neurodynamics. perceptrons and the theory of brain mechanisms. Technical report, CORNELL AERONAUTICAL LAB INC BUFFALO NY, 1961.
- [47] Ammar Nadal Shareef. Simulation of fractal antenna properties composed of metamaterials. https://www.researchgate.net/publication/316106468_Simulation_of_Fractal_Antenna_Properties_Composed_of_Metamaterials/figures?lo=1. Accessed 14th. August, 2018.
- [48] Shiu-Ming Shum and Kwai-Man Luk. Fdtd analysis of probe-fed cylindrical dielectric resonator antenna. *IEEE Transactions on Antennas and Propagation*, 46(3):325–333, 1998.
- [49] SM Shum and KM Luk. Analysis of aperture coupled rectangular dielectric resonator antenna. *Electronics Letters*, 30(21):1726–1727, 1994.
- [50] Jonas Thulin. Machine learning-based classifiers in the direkt profil grammatical profiling system. 2007.
- [51] Vliadimir Vacic. Summary of the training functions in matlab's nn toolbox. *Computer Science Department at the University of California*, 2005.
- [52] WIKIPEDIA. International protection rating. https://en.wikipedia.org/wiki/IP_Code, . Accessed April 30, 2018.
- [53] WIKIPEDIA. Machine learning intro. https://en.wikipedia.org/wiki/Machine_learning#cite_note-4, . Accessed May 1, 2018.
- [54] WIKIPEDIA. Polycarbonate. <https://en.wikipedia.org/wiki/Polycarbonate>, . Accessed 17th. September, 2018.
- [55] WIKIPEDIA. Biological neuron. <https://en.wikipedia.org/wiki/Neuron>, . Accessed 7th. June, 2018.
- [56] WIKIPEDIA. Neuron plasticity. <https://en.wikipedia.org/wiki/Neuroplasticity>, . Accessed 6th. June, 2018.
- [57] WIKIPEDIA. Universal approximation theorem. https://en.wikipedia.org/wiki/Universal_approximation_theorem, . Accessed 11th. June, 2018.
- [58] Qi-Jun Zhang, Kuldip C Gupta, and Vijay K Devabhaktuni. Artificial neural networks for rf and microwave design-from theory to practice. *IEEE transactions on microwave theory and techniques*, 51(4):1339–1350, 2003.
- [59] QM Zhu. A back propagation algorithm to estimate the parameters of non-linear dynamic rational models. *Applied Mathematical Modelling*, 27(3):169–187, 2003.